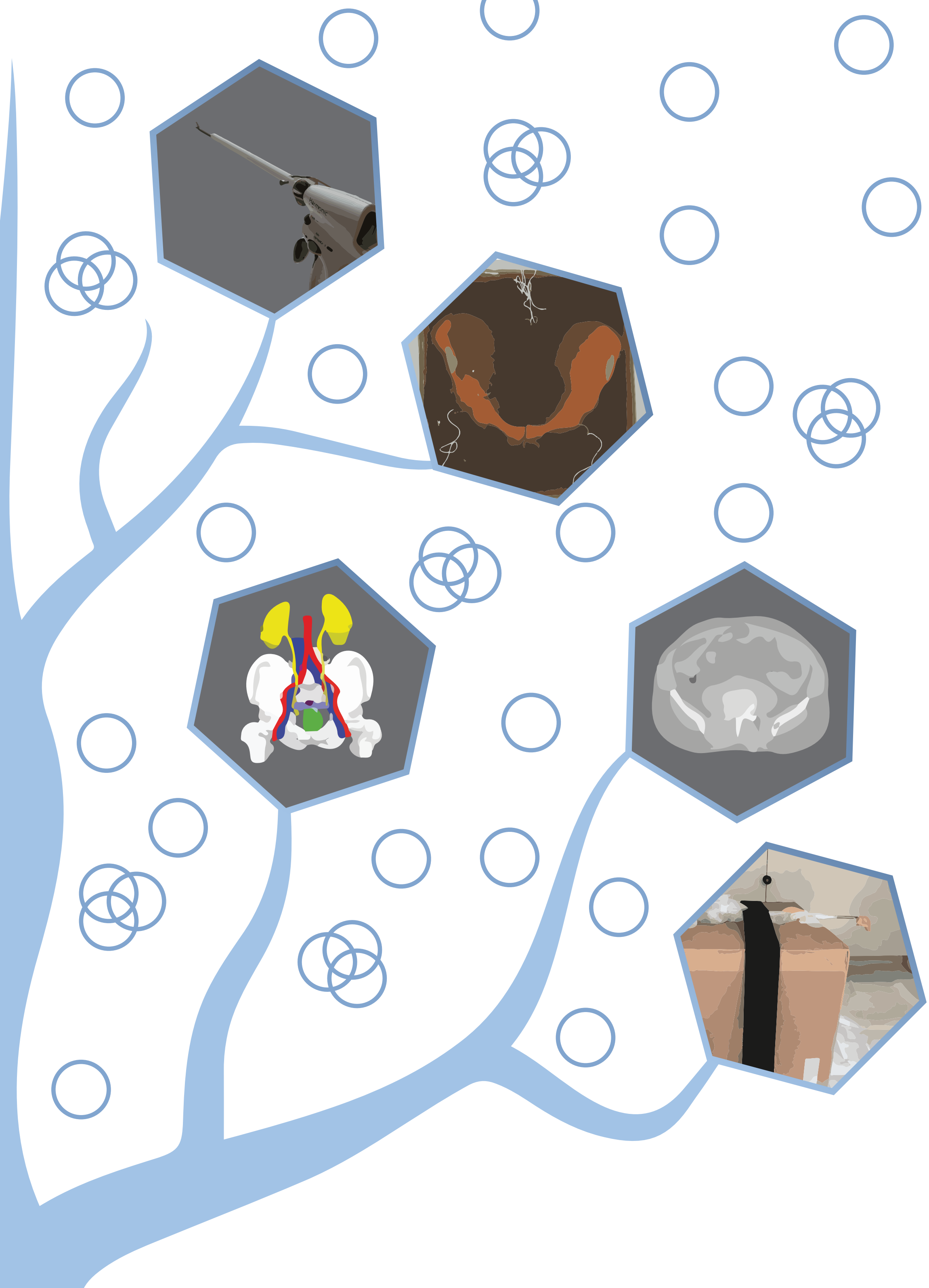

A study into laparoscopic surgical navigation for colorectal cancer patients without a hybrid operating room

L. Noltes

Technical Medicine - Master Thesis

General information

Title	A study into laparoscopic surgical navigation for colorectal cancer patients without a hybrid operating room
Author	L. Noltes
Student Number	s1362321
E-mail	liset.noltes@gmail.com
Date	2nd of September 2019

Organisation

Name	Antoni van Leeuwenhoek - Nederlands Kanker Instituut
Address	Plesmanlaan 121
	1066 CX Amsterdam
Department	Surgical Oncology

University

Name	University of Twente
Address	Drienerlolaan 5
	7522 NB Enschede
Faculty	Science and Technology
Master	Medical Imaging and Interventions

Graduation committee

Chairman	Prof.dr. T.J.M. Ruers
Clinical supervisor	Prof.dr. G.L. Beets
Technical supervisor	Dr.ir. F. van der Heijden
Process supervisor	Drs. P.A. van Katwijk
Additional member	Dr.ir. H.C. Groen
External member	T. Boers, MSc

UNIVERSITY OF TWENTE.

ANTONI VAN LEEUWENHOEK
NEDERLANDS KANKER INSTITUUT

Summary

Background: Surgery or a treatment in combination with surgery is the most common treatment for colorectal cancer. Surgical navigation could alleviate some limitations of laparoscopic surgery. At the Netherlands Cancer Institute - Antoni van Leeuwenhoek (NKI-AvL) a laparoscopic pointer is used for surgical navigation, which cannot be simultaneously inserted thought the trocar with a laparoscopic instrument. Therefore, surgical navigation might not be available all the time. Additionally, the current cone beam computed tomography (CBCT) registration exposes the patient and medical personal to radiation during the CBCT and makes surgical navigation limited available at the NKI-AvL and other hospitals. In this thesis, the clip-on, which integrates an electromagnetic (EM) sensor and the Ethicon Harmonic ACE (EH-ACE) into one device is evaluated, and the accuracy of 3D tracked ultrasound (US) registration for abdominal surgical navigation is compared to the current CBCT registration.

Clip-on: The EM sensor is not exactly located at the tip of the disposable EH-ACE when using the clip-on. Four clip-on calibrations were evaluated on accuracy. The results show a clip-on calibration where only a single clip-on/EM sensor/EH-ACE combination is calibrated, which can be used with any clip-on and any EH-ACE with that specific EM sensor. Thereafter, the accuracy inside the entire table top field generator workfield is evaluated using 112 points of interest. The results show an root mean square error of 2 mm, with a significant difference ($p = 0.004$) of 0.2 mm when another EM sensor was used, which was not deemed clinical relevant. Surgical navigation can also be used during activation of the EH-ACE, because activation of the EH-ACE does not seem to influence the accuracy of tracking with the clip-on. Recommendation to further improve the design of the clip-on was made.

Registration with 3D tracked ultrasound for abdominal surgical navigation: The target registration error (TRE) of 3D tracked US registration was compared to the CBCT registration for abdominal surgical navigation in a phantom study. The results show a comparable TRE for 3D tracked US registration and CBCT registration, when the segmented left and right iliac crest together with the os pubis were used for registration. Sweeping the US beam to fast over the anatomy must be prevented, because gaps in the segmentation negatively influence the registration results. Pre-processing of the data might be a solution when only left and/or right iliac crest segmentation are used for the registration with 3D tracked US. Before clinical implementation further research is necessary, especially focused on bone segmentation in US imaging.

Preface

This thesis is the result of my master graduation internship for the specialisation Medical Imaging and Interventions of the master Technical Medicine at the University of Twente. I enjoyed my ten months internship at the department surgical oncology at the Nederlands Kanker Instituut - Antoni van Leeuwenhoek, were I worked on this graduation research and my clinical development. I welcome this opportunity to thank everyone who contributed to the realisation of this thesis.

First, I would like to thank my supervisors. I am grateful that I could always approach you with questions and that you encouraged me to reach my goals. Harald, I was lucky to have you as my weekly supervisor. Thanks for your guidance, brainstorm sessions, you confidence and that I could always express my ideas. Your curiosity and critical eye sometimes challenged me, kept me motivated and helped me to lift this thesis to the next level. I want to thank Geerard Beets for the clinically supervision and constructive consultation. Ferdi, thank you for the efficient and fruitful technical meetings, you challenged me in becoming a better researcher. I want to thank Paul for the 'intervisie' meetings. You know how to hit a nerve with your sharp questions, which helped me to grow personally and as a Technical Physician. Theo, thank you for always being critical during the research meetings and for being my chairman. I want to thank Tim Boers for being my external member at my graduation committee.

I would like to thank my colleagues; Freija, Huib, Lars, Lotte, Luuk, Roeland, Sharmana, Stephan and Wouter for all the walks, coffee breaks and vrimibo's. You made my internship a lot more fun. I also want to thank Sandra Wagenvoort for her tireless dedication towards all the students at the surgical oncology department.

I would like to thank Bastet, Cascade and my big crazy family for being my safety net. A special thanks to my lovely friends Bernice, Lieke and Marijn. The hard work during the study bloomed into a priceless friendship. Thank you for the teamwork, coffee breaks, support, celebrating exam week with cake, stupid jokes and the big amount of fun we had. Without you it would not have been the same.

A special and grateful thanks to Jan, Annie, Erik and Timon, for your positive energy, advice and confidence in me. You let me look at the bright side of graduation. Timon without your unconditionally support, I would not be here, at the finish line of my graduation. I love your positive perspective and your 'het komt allemaal wel goed'. I am forever grateful that I could always come to you, that you are always there for me and that you bring out the best in me.

Liset Noltes
Utrecht, August 2019

List of abbreviations

2D	Two-dimensional
3D	Three-dimensional
5DOF	Five degrees of Freedom
6DOF	Six degrees of Freedom
ANOVA	Analysis of variance
CBCT	Cone beam computed tomography
CT	Computed Tomography
EH-ACE	Ethicon Harmonic ACE
EM	Electromagnetic
EMTS	Electromagnetic tracking system
FRE	Fiducial registration error
G11 Endo-surgery	Ethicon Harmonic G11 Endo-surgery Generator
IQR	Interquartile range
MRI	Magnetic resonance imaging
NKI-AvL	Netherlands Cancer Institute - Antoni van Leeuwenhoek
OTS	Optical tracking system
RMSE	Root mean square error
SCU	System control unit
SIU	System interface unit
TRE	Target registration error
TTFG	Table top field generator
US	Ultrasound

Contents

Introduction 1

1.1 Clinical Background

1.1.1 Colorectal cancer

Colorectal cancer is the second most commonly occurring cancer in woman and the third most commonly occurring cancer in men worldwide [1]. The Netherlands are ranked at the tenth place for the incidence rate of colorectal cancer in 2018 worldwide [1]. The incidence of colorectal cancer has increased over the past decades in the Netherlands [2]. A total of 14000 new patients were diagnosed with colorectal cancer in the Netherlands in 2018, which equals to 84 cases per 100,000 residents [2]. Colorectal cancer arises in a small number of mucosal polyps through the adenoma-carcinoma sequence. Adenomatous colorectal polyps are a abnormal growth of cells, very common and usually asymptomatic. A small number can become malignant, this is a slow process of approximately 10 to 15 years [3]

Anatomy

The colon starts in the right lower quadrant of the abdomen, were the contents of the small intestine enter the colon through the ileocecal valve. Thereafter, it continues as the ascending colon. The ascending colon turn into the transverse colon, which crosses the midline, and continues as descending colon and sigmoid colon to the rectum and anal canal, see Figure 1.1a. The pelvic cavity is bounded by bony structures. The two hip bones are located at the lateral and anterior side and the sacrum and coccyx at the posterior side, see Figure 1.1b. The two hip bones are formed by the following three parts: ilium with iliac crest, os pubis and os ischii.[4].

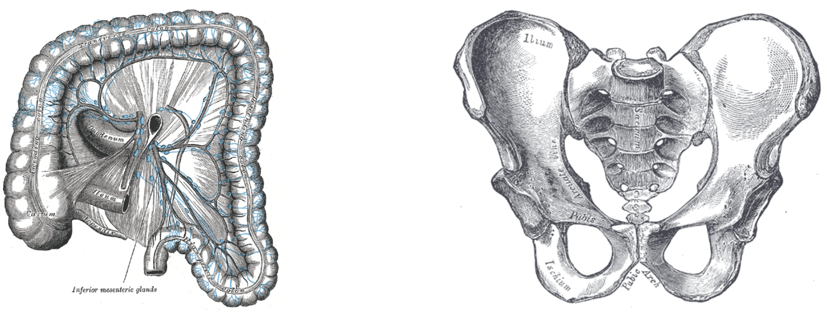

(a) Colon **(b)** Pelvic bones

Figure 1.1: Anatomy [4]

Diagnosis colorectal cancer

The most important symptoms of colorectal cancer are: blood in faeces, rectal bleeding, change of bowel habit, abdominal pain, unintended weight loss and fatigue/weakness [5], [6]. Genetic factors are another important prediction of colorectal cancer [6], [7]. Usually, the symptoms do not appear until the disease is relatively advanced and the symptoms are often ignored by patients [8]. In the Netherlands, the health authorities introduced a national screening program since 2014 [9]. The screening program consist of a faecal occult blood test. The faecal occult blood test has a sensitivity of 40% and a relatively low specificity [8]. The screening can detect malignant tumours and polyps. Additional examination is needed after a positive test, due to the low specificity. Colonoscopy is the preferred technique to establish the diagnosis of a colorectal carcinoma [10]. Computed tomography (CT) colography is recommended, when colonocopy is not possible or unable to detect the tumour [2], [8], [9]. The staging for local extent of the disease and distant metastases is usually performed with CT, and magnetic resonance imaging (MRI) for the local staging of rectal tumours [2], [8], [9].

Colorectal cancer has five different stages [11], see Figure 1.2

- Stage 0; carcinoma in situ. The cancer cells are strictly confined to the mucosa and are not invading. There is no risk for metastases and this stage is considered a pre-malignant stage.
- Stage 1. The cancer is confined to the mucosa or muscularis of the wall of the colon or rectum.
- Stage 2. The cancer has grown through the muscular wall of the colon or rectum.
- Stage 3. The cancer has has spread to locoregional lymph nodes.
- Stage 4. The cancer has spread to other parts of the body (metastasis).

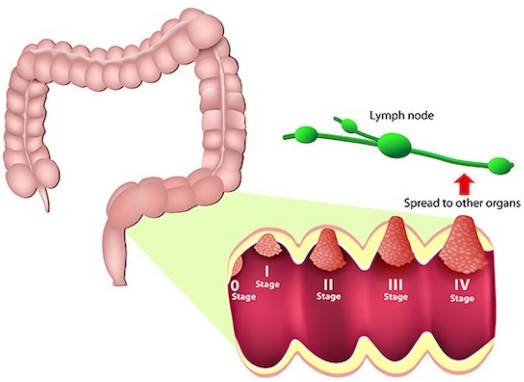

Figure 1.2: The five different stages of colorectal cancer [12]

Treatment colorectal cancer

The four mean treatment options for colorectal cancer are: polypectomy and local excision, surgical resection of a segment of bowel, chemotherapy, radiotherapy or a combination [2]. The choice of the treatment depends on the stage of the colorectal cancer [2]. Surgery, or a treatment in combination with surgery, is the most common treatment [2]. The segment of colon with the tumour is removed together with the mesentery, the feeding blood vessels and lymph nodes. This is traditionally performed by open surgery, through a laparotomy, but is now increasingly performed laparoscopically, because of the decreased surgical trauma and a the associated improved postoperative quality of life outcomes [13]–[16]. Laparoscopic colorectal surgery shows a lower estimated blood loss, shorter hospital length of stay, less pain and lower hospital costs compared to open surgery [14], [17]–[22].

1.1.2 Laparoscopic surgery

Several small incision are made to allow trocar placement as a means of access for the camera and instruments to the abdomen. A working space is made by inflating the abdominal cavity with carbon dioxide gas, creating a pneumoperitoneum. However, the pelvic space is fixed, due to the bony structures, creating a limited working space for surgery in the pelvis. Usually, there is one active device to dissect and cut the tissue, and one or more assisting instruments for retraction and exposure. All the movements of the laparoscopic instruments inside the abdominal cavity are captured by the laparoscopic camera and projected on 2D screens in the operating room.

1.1.3 Clinical Problem

Viewing the surgical site through the camera on 2D screens causes difficult depth perception [23]. Additionally, the use of laparoscopic instruments causes reduced tactile feedback compared to open surgery [24]. Certain anatomical landmarks can disappear from the view, when the camera focuses on a smaller field. This challenges locating the tumour in relation to the laparoscopic instrument. Surgical navigation is a technique that can show the live position and orientation of surgical instruments in relation to anatomical structures and tumour(s) visible on preoperative imaging. Using this technique in laparoscopic surgery could alleviate some of the limitations, consequently possibly improving the accuracy and efficacy of the procedure.

1.2 Abdominal Surgical Navigation

1.2.1 Electromagnetic and optical tracking

The two main tracking methods used for surgical navigation are electromagnetic (EM) tracking and optical tracking. The electromagnetic tracking system (EMTS) uses an EM sensor and the optical tracking system (OTS) uses a retro reflecting marker, to determine the position and orientation of surgical instruments in relation to anatomical structures. Whereas the EM sensors are wired, the OTS markers are wireless and dependent on a direct line of sight [25], [26]. This is not the only difference between EMTS and OTS. The OTS has a higher accuracy compared to EMTS [26], [27]. Furthermore, ferromagnetic materials can influence the accuracy of the ETMS by creating eddy currents [26], [28], [29]. There is no direct line of sight to the tip of the laparoscopic instrument in the abdominal cavity during laparoscopic surgery. Therefore, a OTS marker should be placed at the handle. The position and orientation error increases with a larger distance to the tip of the laparoscopic instrument, known as lever arm effects [26]. EM sensors placed at the tip of the surgical instrument provides a higher accuracies compared to OTS markers placed at the handle of the instrument [26]. Furthermore, a clear line-of-sight between the handle of the laparoscopic instrument and the optical tracking device is difficult in a surgical setting due to the present equipment and medical personnel. Concluding, EMTS is preferred during laparoscopic colorectal surgical oncology.

At the Netherlands Cancer Institute - Antoni van Leeuwenhoek (NKI-AvL), the Aurora V2 (Nothern Digital Inc., Waterloo, Cananda) EMTS is available, consisting of a tabletop field generator (TTFG) and various EM sensors.

1.2.2 Tabletop field generator

The TTFG generates an oval magnetic workfield of 600x420x600 mm where EM tracking is possible with a measurement rate of 40 HZ [30], [31]. No EM data can be acquired in the first 120 mm above the TTFG. The workfield where surgical navigation can take place and the axes of the related coordinate system are visualised in Figure 1.3

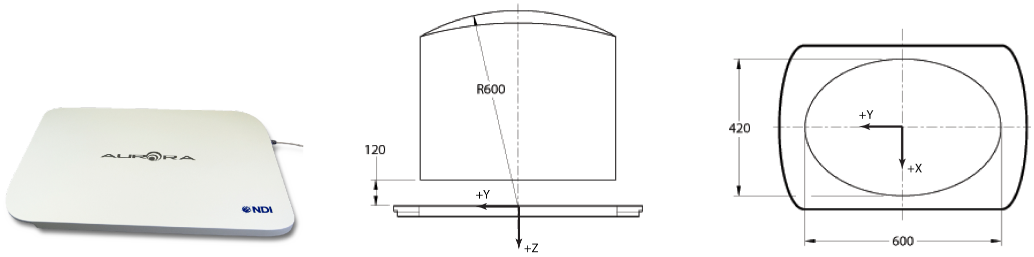

(a) TTFG [32] **(b)** Workfield TTFG, yz-plane [31] **(c)** Workfield TTFG, xy-plane [31]

Figure 1.3: The NDI Aurora tabletop field generator (TTFG)

1.2.3 Electromagnetic tracking sensors

EM sensors consist of small coils. A current is induced, when the EM sensor is introduced in the workfield of the TTFG. The EM sensors are connected to a system interface unit (SIU, Figure 1.4a), which amplifies the electrical signal. The SIU is connected to the system control unit (SCU, Figure 1.4b), which calculates the position and orientation of the EM sensor in relation to the TTFG. The NKI-AvL has two SIU connected to one SCU. Therefore, at most eight EM sensors can be tracked simultaneously.

(a) SCU. **(b)** SUI.

Figure 1.4: The system control unit (SCU) and the system user interface (SUI) [31]

There are two types of EM sensors, a five degrees of freedom (5DOF) and a six degrees of freedom (6DOF) sensors. The 5DOF EM sensor provides three positions (x,y,z) and two orientations (pitch, yaw), while the 6DOF EM sensor provides an additional orientation, the roll (1.5). The position accuracy for 5DOF and 6DOF EM sensor seems to be equal [33]. For both 5DOF and 6DOF, the position and orientation accuracy decreases, with increasing distance between the EM sensor and TTFG [33].

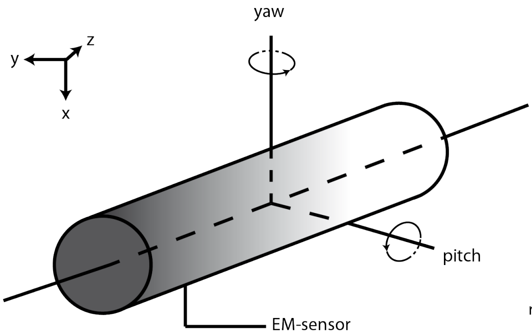

(a) 5DOF EM sensor

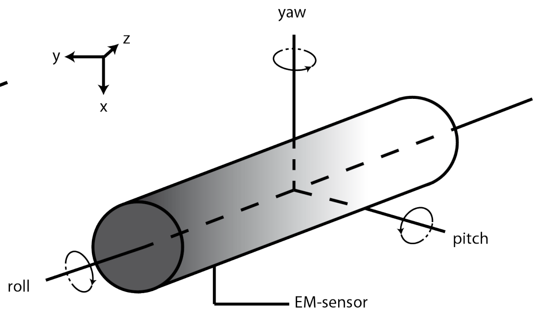

(b) 6DOF EM sensor

Figure 1.5: Schematic overview of two electromagnetic (EM) sensors. Both five degrees of freedom (5DOF) and six degrees of freedom (6DOF) EM sensors provide the x-, y- and z-position and two orientations pitch and yaw. Additionally, the 6DOF provides a third orientation, the roll.

Important to note; The 5DOF EM sensor used in this thesis is the Philips 5DOF Patient Sensor, which actually consists of two 5DOF EM sensors. The Philips 5DOF Patient Sensors are produced by Northern Digital Inc., but medical certified and distributed by Philips. The 6DOF EM sensors used in this thesis are the Aurora 6DOF Cable Tool, Aurora Micro 6DOF Sensor, Aurora 6DOF Probe and the 6DOF laparoscopic pointer, see Figure 1.6.

(a) Philips 5DOF Patient Sensor

(b) Aurora 6DOF Cable Tool

(c) Aurora Micro 6DOF Sensor

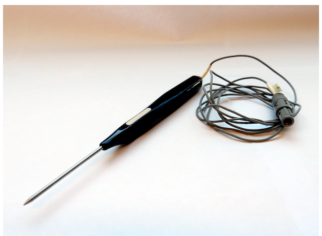

(d) Aurora 6DOF Probe

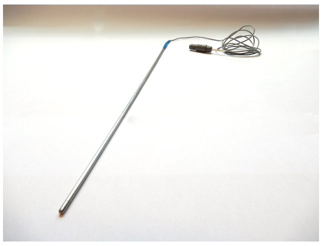

(e) 6DOF laparoscopic pointer

Figure 1.6: The electromagnetic tracking sensors. Abbreviations: 5DOF, five degrees of freedom; 6DOF, six degrees of freedom

Limitations

A laparoscopic pointer with a 6DOF EM sensor embedded in the tip was developed at the NKI-AvL. The pointer is applied in ongoing studies of navigated colorectal surgeries at the NKI-AvL. The laparoscopic instruments and the laparoscopic pointer cannot simultaneously be inserted through a trocar. Therefore, the laparoscopic pointer and a laparoscopic instrument take turns going through the trocar. Consequently, the surgeon needs to remember where the laparoscopic pointer indicated important anatomical structures and tumour tissue, resulting in a lower accuracy. Furthermore, the laparoscopic pointer might not always be inside the workfield of the tabletop field generator. Consequently, surgical navigation might not be available all the time. Therefore, a clip-on was developed, which integrates a 6DOF EM sensor and a laparoscopic instrument into one device.

Clip-on

The clip-on needs to be developed to integrate a 6DOF EM sensor and a laparoscopic instrument into one device. The laparoscopic colorectal surgeon uses two laparoscopic instruments simultaneously, an 'assisting' laparoscopic instrument and an 'active' laparoscopic instrument. The assisting instrument is used for retraction and exposure, to create a clear overview regarding the target tissue. The active instrument is used to dissect and cut the tissue. This one has more possibilities to freely move around, as an 'assisting' laparoscopic instrument is often required to create a clear overview. The possibility to freely move around is favourable for surgical navigation, because in that case the surgeon can point to anatomical structures. A disposable ultrasonic or diathermy instrument is most of the time used as the 'active' laparoscopic instrument during colorectal surgery. In consultation with the colorectal laparoscopic surgeons in of the NKI-AVL it is decide to first develop a clip-on for the Ethicon Harmonic ACE (EH-ACE).

The EH-ACE is a vessel sealing device that uses ultrasonic technology. Ultrasonic technology transforms electrical energy to mechanical energy in the form of vibrations [34]. The vibrations in the tip of the EH-ACE causes heat, therefore vessels can be coagulated and cut. The EH-ACE is available in two different versions; the EH-ACE 7+ Shears and the EH-ACE+ Shears (1.7). The EH-ACE 7+ Shears has three activation buttons, minimal, maximal and advanced hemostasis, whereas the EH-ACE+ Shears has two activation buttons, the minimal and maximal activation. The maximal activation is for sealing the smaller vessels, the minimal activation for sealing vessels up to 5 mm and the advanced hemostasis enables more precise delivery of the energy [35].

The surgeon needs to navigate through the limited working space in the pelvic area and requires a clear view on of the tip of the EH-ACE. Therefore, the 6DOF EM sensor is placed at a certain distance from the tip. The EMTS can only track the EM sensors and thus does not directly track the tip of the EH-ACE. Therefore, the tip-offset between the EM sensor and the EH-ACE needs to be determined, using a

(a) EH-ACE 7+ Shears [35].

(b) Handle EH-ACE 7+ Shears [36].

(c) Handle EH-ACE+ Shears [37].

Figure 1.7: The Ethicon Harmonic ACE (EH-ACE) 7+ Shears (a) looks almost exactly the same as the EH-ACE+ Shears. The small difference on the outside in located in the handle. The handle of the EH-ACE 7+ Shears (b) contains the buttons maximal, minimal and advanced hemostasis, while the handle of the EH-ACE+ Shears (c) contains the buttons maximal and minimal activation.

calibration. In this thesis, the term that will be used to describe this phenomenon is 'clip-on calibration'.

Clip-on calibration

The manufacturing accuracy might influence both the dimensions of the EH-ACE and clip-on. As the calibration will be done for the specific dimensions of a EH-ACE and clip-on combination, a variation in these dimensions resulting from a different combination of EH-ACE and a clip-on could influence the accuracy of tracking. Therefore, different combinations of EH-ACE and clip-on will be calibrated and evaluated on accuracy and ease-of-use.

Accuracy

Before a clinical tool can be applied in clinical practice, the accuracy and reproducibility of the system needs to be evaluated. The surgeon needs to know that tracking with the clip-on is accurate inside the entire TTFG workfield and that this accuracy stays similar when the sensor needs to be replaced. Furthermore, the activation of an ultrasonic device might influence the accuracy of the tracking. The extent of influence and if this is time-based will be evaluated. All these subjects will be examined in chapter 2 Clip-on.

1.2.4 Registration for abdominal surgical navigation at the NKI-AvL

In-house developed software

During surgical navigation, the live position and orientation of a surgical instrument, for example the Aurora 6DOF Probe, is visualised in relation to anatomical structures on pre-operative imaging together with a three-dimensional (3D) model. Multiple in-house software packages were developed to accomplish this task. Two of these will be used throughout this thesis and will be further elaborated. First, WorldMatch, is used for the creation of the 3D model. Important anatomical structures and tumour(s) are semi-automatic segmented and used to build the three-dimensional (3D) model, see Figure 1.8. To simplify the segmentation, an overlay of CT, cone beam computer tomography (CBCT), MRI and PET-CT could be created. Second, SurgNav, is used as surgical navigation software in combination with the EMTS, which is currently applied in lower jaw, liver, lymph node and rectal surgery. The software accommodates a four-display mode (axial, sagittal, frontal and 3D model) where position and orientation of the EM sensor is visualised on the pre-operative imaging [38], see Figure 1.8. Besides that, SurgNav is able to create a overlay between different imaging modalities, just like WorldMatch.

Current Workflow

The current workflow to enable surgical navigation can be divided in two phases, the preoperative planning and the intraoperative phase, see Figure 1.8.

During the preoperative planning two CT-scans, an arterial phase CT-scan and a washout CT-scan, are acquired. These scans are used, together with other available imaging modalities, to create the 3D model using WorldMatch. Before the operation, the TTFG is placed in a specially designed carbon surgical table, whereupon the patient is positioned. During surgical navigation the live position and orientation of a surgical instrument needs to be shown in relation to the anatomy of the patient. Therefore, the EMTS, which tracks surgical instruments using EM sensors and the pre-operative CT imaging, which show the anatomy of the patient must be linked together. Corresponding points between EMTS and pre-operative CT can be used for this registration. In the current situation this is done by Philips 5DOF Patient Sensors (Figure 1.6), which are visible on the CT imaging and have an EMTS signal. The patient EM sensors cannot be placed during the pre-operative CT imaging, because skin movements and the difference in position, straight legs during the CT-scan and French position in the operating room, can cause inaccuracies [38]. Therefore, the EM sensors are placed just before the start of the operation at the lumbar curvature left and right of the spine and on the pubic bone. The patient is sedated, positioned

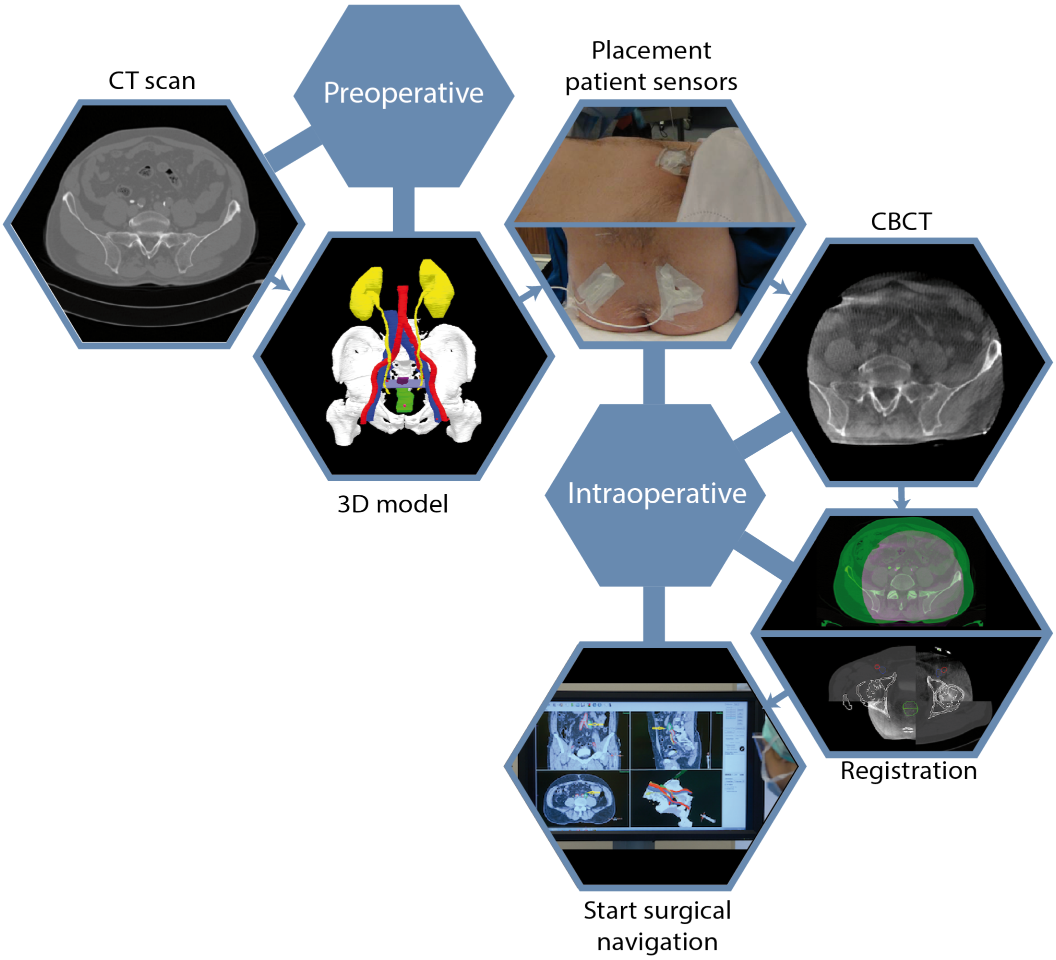

Figure 1.8: Preoperative and intraoperative phase of the surgical navigation.

and a cone beam computed tomography (CBCT) imaging (Philips Allura FD20 XperCT) of the pelvic bones and the Philips 5DOF Patient Sensors are acquired. The image resolution of the CBCT is lower compared to the pre-operative CT, but can be used to link the EMTS and pre-operative CT with help of registrations in SurgNav. Thereafter, the surgical navigation can start.

Registration with CBCT

As explained above, the CBCT is used to link the EMTS and pre-operative CT, with help of two registrations, see Figure 1.9. First, CBCT-system and CT-system are registered with help of the bones on the CBCT imaging and the bones on the preoperative CT imaging. SurgNav allows bone-bone registration between CT and CBCT imaging. The best matching rotation matrix (${}^{CT}\mathbf{R}_{CBCT}$) and translation vector (${}^{CT}\mathbf{t}_{CBCT}$) are saved into a transformation matrix (${}^{CT}\mathbf{T}_{CBCT}$), see Eq. 1.1. Second, the EM-system and the CBCT-system are registered, with help of the patient EM sensors, which are imaged by the CBCT and visible by the EMTS. The centre of the patient EM sensors imaged on the CBCT are determined (${}^{CBCT}\mathbf{p}$) Thereafter, the position of the patient EM sensors expressed in the EM-system (${}^{EM}\mathbf{p}$) are acquired by

SurgNav and the fiducial registration is executed. The best matching rotation matrix ($^{CBCT}\mathbf{R}_{EM}$) and translation vector ($^{CBCT}\mathbf{t}_{EM}$) is saved into a transformation matrix ($^{CBCT}\mathbf{T}_{EM}$), see Eq. 1.2.

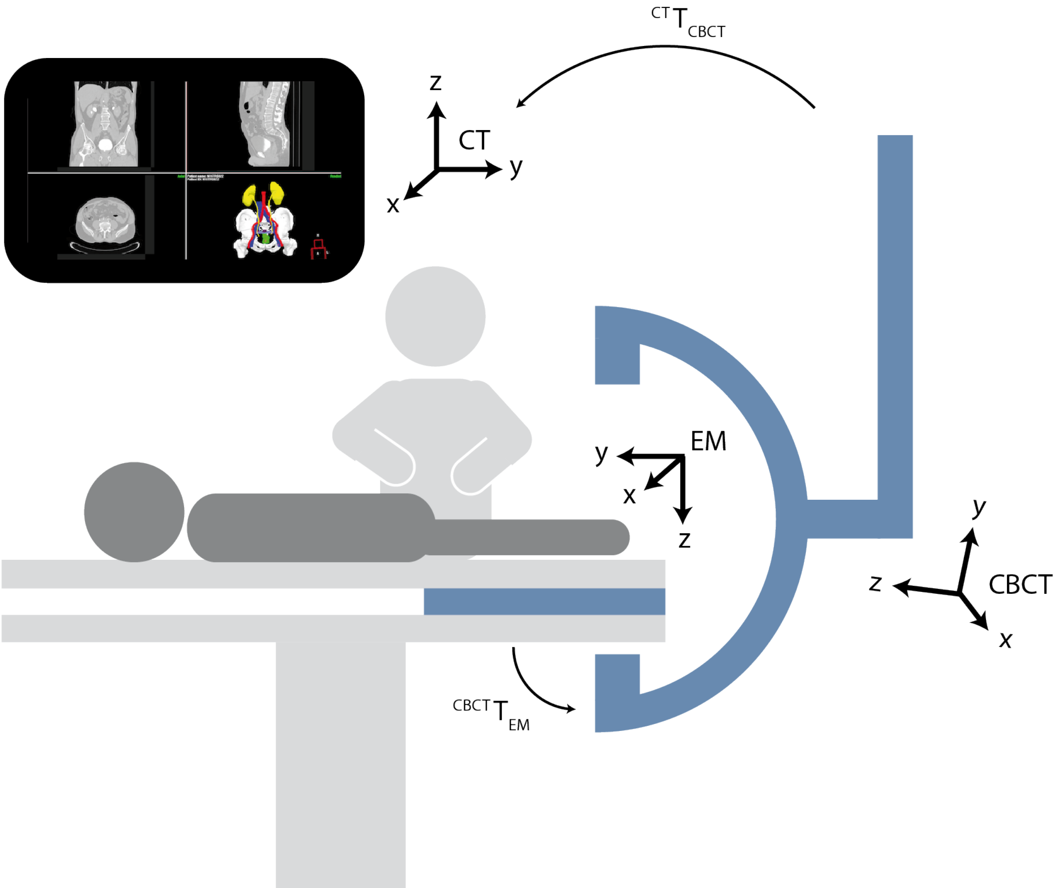

Figure 1.9: Schematic overview of the operating room set-up and the coordinates systems from different components during surgical navigation using CBCT.

$$^{CT}\mathbf{p} = ^{CT}\mathbf{R}_{CBCT}\ ^{CBCT}\mathbf{p} + ^{CT}\mathbf{t}_{CBCT} = ^{CT}\mathbf{T}_{CBCT}\ ^{CBCT}\mathbf{p} \tag{1.1}$$

$$^{CBCT}\mathbf{p} = ^{CBCT}\mathbf{R}_{EM}\ ^{EM}\mathbf{p} + ^{CBCT}\mathbf{t}_{EM} = ^{CBCT}\mathbf{T}_{EM}\ ^{EM}\mathbf{p} \tag{1.2}$$

Consequently, the transformation matrix from CBCT-system to CT-system ($^{CT}\mathbf{T}_{CBCT}$) and the transformation matrix from EM-system to CBCT-system ($^{CBCT}\mathbf{R}_{EM}$) is known, therefore the transformation matrix from EM-system to CT-system ($^{CT}\mathbf{T}_{EM}$) can be calculated, see Eq. 1.3. When an EM sensor is introduced in the TTFG workfield after these two registrations, then the EM sensor will be visualised in relation to the anatomical structures with help of the coronal, sagittal and transverse CT imaging planes and a 3D view with a 3D model, see Figure 1.9.

$$^{CT}\mathbf{T}_{EM} = ^{CT}\mathbf{T}_{CBCT}\, ^{CBCT}\mathbf{T}_{EM} \tag{1.3}$$

Limitations

The main limitation of this workflow is the dependency on the CBCT, see Figure 1.8 and Figure 1.9. The CBCT is limited available in the NKI-AvL, because there is only one operation room with a CBCT. A solution might be to move the patient to another operation room after the CBCT, so the CBCT is available for another patient. However, this causes inaccuracies, due to movements of the EM sensors in relation to the bone, when the patient moves to another operating table. Consequently, surgical navigation is limited available in the NKI-AvL. Besides that, patients and medical personals are exposed to radiation during the CBCT, or the medical personal need to leave the operation room, which costs time. Furthermore, when surgical navigation will be expanded to other hospitals, a hybrid OR with a CBCT is required, limiting the number of hospitals tremendously. Consequently, surgical navigation would be limited available in other hospitals. That is why there is a high demand for an alternative registration method.

For the alternative registration method it is important to make use of a rigid structure, that has the same morphology on the pre-operative CT scan as at the patient set-up in the operating room. Furthermore, the registration method needs to be able to link the EMTS to the pre-operative CT imaging. The abdomen and pelvic area consists mostly of non-rigid structures, making it a challenging area for registration. The hip bones are the most rigid structures in the pelvic area. Therefore, it is important that the new registration technique enables a rigid bone registration. The research in this thesis examines if 3D tracked ultrasound (US) registration is a good alternative for the CBCT registration. So, surgical navigation will also be available without a hybrid operating room and medical personal and patients will not be exposed to radiation.

Registration with 3D tracked ultrasound

As stated before, it is important to use the rigid bone in the pelvic area to link the EMTS system, patient set-up to pre-operative imaging. Cortical bone has a high acoustic impedance of $4 \cdot 10^6$ up to $8 \cdot 10^6$ $kg \cdot s^{-1} \cdot m^{-2}$ compared to water, fat and muscle [39]. The high acoustic impedance of the bone surface causes a high reflection of the US wave, resulting in a high intensity on the B-mode US imaging. Consequently, almost no US waves enter the area underneath the bone surface, resulting in a 'shadow region' with low intensities on the B-mode US imaging, see Figure 1.10a.

The US images of the bone can be acquired with the BK medical US system (bk5000) and T-shaped intraoperative transducer (I14C5T). The transducer has a focal range of 10 up to 80 mm, which makes it possible to image the iliac crest, ilium and os pubis. It is important to know where the US images are located in the EMTS coordinate system, so the patient set-up and ETMS system can be linked to the pre-operative imaging. Therefore, a holder with a 6DOF Cable tool inside was designed, which clasps on the transducer, see Figure 1.10b. An intrinsic calibration between the 6DOF cable tool and images was performed following the calibration method of Lars Eirik Bø et al 2015, the root mean square error (RMSE) of the tracking was determined at 1.5 mm in the NKI AVL [40]. The TTFG is located below the patient during 3D tracked US. The transducer acquires two-dimensional (2D) US images, while the 6DOF cable tool acquires the position and orientation of the probe. Consequently, the 2D images can be reconstructed into a 3D volume with help of the software CustusX (SINTEF, Trondheim, Norway), see Figure 1.10c

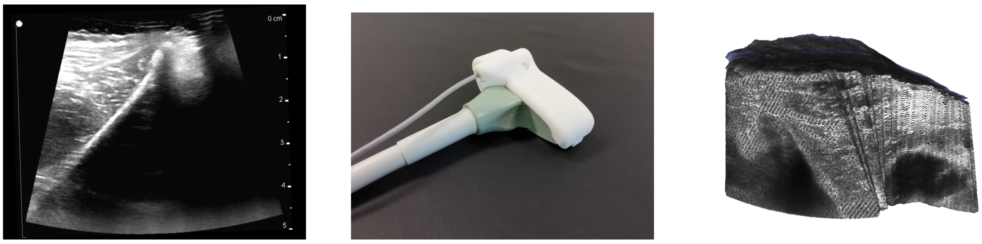

(a) 2D US image with shadow region **(b)** T-shaped intraoperative transducer with clasp **(c)** 3D US volume

Figure 1.10: The three-dimensional (3D) ultrasound (US) volume (c), consists of stacked two-dimensional (2D) US images (a) acquired by the T-shaped operative transducer with clasp (b)

Target registration error

For clinical implementation it is important to know how registration with 3D tracked US performs. A frequently used approach to evaluate the accuracy of the registration, is to calculate the target registration error (TRE). Two sets of corresponding points are selected in two registered volumes. It is important that the points for the calculation of the TRE did not contribute to the registration. First, the ED between two corresponding points and thereafter the RMSE of the points is calculated.

Currently, very little is known about the TRE of the 3D tracked US registration during surgical navigation. The TRE of the current workflow, with CBCT registration is 4.0 mm [38]. In this thesis a workflow for the 3D tracked US registration is provided, where the TRE is compared to the current workflow using CBCT.

1.2.5 Objectives

In this study, a new workflow is proposed and evaluated enabling laparoscopic surgical navigation for colorectal cancer patients without using a hybrid operating room.

Research question one:
Which clip-on calibration method must be used for the clip-on?

Research question two:
What is the accuracy and reproducibility of the clip-on inside the TTFG workfield?

Research question three:
Does activation of the Ethicon Harmonic ACE influence the accuracy of tracking with the clip-on?

Research question four:
What is the accuracy of abdominal surgical navigation using tracked 3D ultrasound compared to using CBCT?

2 Clip-on

2.1 Clip-on improvement

A previous project focused on the design of the clip-on [41]. The clip-on consists of two parts: a sensor holder, and a sleeve to fit over the EH-ACE 7+. This two part set-up was chosen, so both parts can be replaced independently from each other. The sensor holder prevents translation and rotation of the EM sensor. The sleeve has a docking part which connects to the base of the EH-ACE ensuring that the sleeve and EH-ACE have the same rotation. The sleeve is fixated in translation by a blunt screw. Inside the sleeve is a tunnel and a cut-out to incorporate the sensor cord and holder. This cut out is approximately 12 cm from the tip of the EH-ACE 7+. In this way, the surgeon always has a clear view on the tip. Furthermore, the shaft of the EH-ACE 7+ near the tip remains thin, aiding navigation through the limited working space in the pelvic area. Fused deposition modelling with polylactic acid and Ultimaker3 was used for the production of the clip-on prototype. However, this has some limitations: post processing was required, the product contained irregularities and the material was not reusable.

In consultation with the head of infection prevention and sterilisation department it is decided to use Nylon PA2200 with ISO Certificate 13485 and selective laser sintering for the production of the clip-on. This technique does not need post processing and the material could be cleaned, sterilised and can therefore be reused. The Aurora 6DOF Cable Tool is glued into the sensor holder with Nusil silicone adhesive. The clip-on used in this thesis is visualised in Figure 2.1

2.2 Clip-on calibration

2.2.1 Introduction

As explained earlier, the 6DOF cable tool is located approximately 12 cm from the tip, when the clip-on is attached to the EH-ACE. Furthermore, the manufacturing accuracy might influence both the dimensions of the EH-ACE and the clip-on. Therefore, different combinations of EH-ACE and clip-on will be calibrated during this

(a) Holder; and 6DOF Cable Tool

(b) Sleeve; integrates the 6DOF Cable Tool with the EH-ACE 7+ Shears

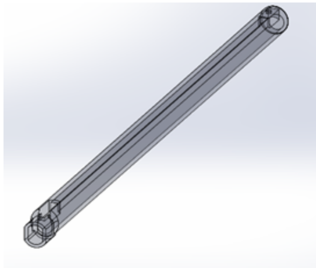

(c) Wireframe of the sleeve

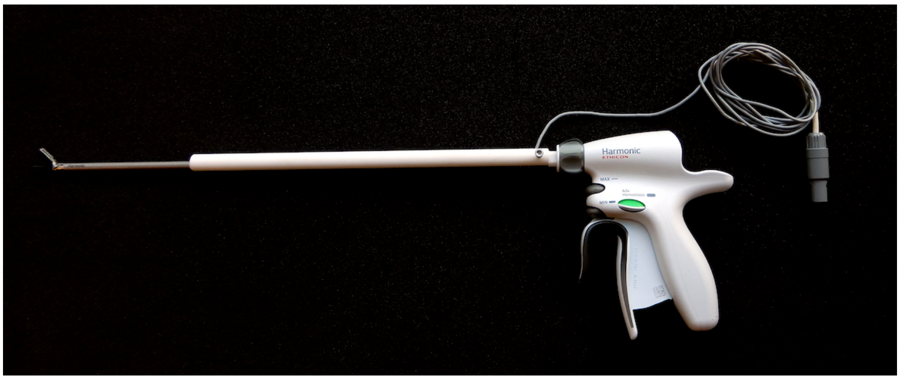

(d) Ethicon Harmonic ACE 7+ with clip-on. Abbreviations; 6DOF, six degrees of freedom

Figure 2.1: Different parts of the clip-on

experiment. These combinations will be evaluated on the overall accuracy and ease-of-use. There are three clip-on calibration options:

1. Individual calibration.
   Each unique clip-on/sensor/EH-ACE combination is calibrated, which can only be used for that specific set
2. Pair calibration.
   Each unique clip-on/sensor pair is calibrated individually, which can be used with any EH-ACE
3. Generic calibration.
   Only one clip-on/sensor/EH-ACE is calibrated, which can be used with any clip-on and any EH-ACE.

The different clip-on calibration options will be evaluated on overall accuracy. The final choice which clip-on calibration will be used, is not only dependent on the accuracy, as the ease-of-use in clinical practice is also of great importance. The EH-ACE is a disposable laparoscopic instrument. Therefore, choosing the individual calibration requires that the clip-on calibration is performed in the sterile environment of the OR, just before the start of the surgical procedure, which might cause a longer surgery time. Pair calibration and generic calibration does not require the calibration to be performed in a sterile environment, because the calibrated clip-on can be recombined with another sterile EH-ACE.

2.2.2 Materials and Methods

Materials

- Tabletop field generator (V2 System, Northern Digital Inc., Waterloo, Cananda)
- Aurora 6DOF Probe (straight tip, standard, NDI 610065)
- Aurora 6DOF Cable Tool (diameter=2.5 mm, length = 2000 mm, NDI 610016)
- Philips 5DOF Patient sensor
- NDI Architect (Northern Digital Inc. Toolbox Software for pivoting)
- SurgNav (in-house developed software for surgical navigation)
- Three Ethicon Harmonic ACE 7+ Shears (HARH36, shaft length = 360 mm, diameter=5 mm)
- Two Ethicon Harmonic ACE+ Shears (HAR36, shaft length = 360 mm, diameter=5 mm)
- Four clip-on
- Clip-on calibration phantom (diameter divot = 1 mm)
- Pyramid phantom (diameter divots = 6 mm, 8 mm and 10 mm)
- CT-scan pyramid phantom (slice thickness = 0.6 mm, pixel spacing = 0.66 mm)
- Non-ferromagnetic spacer (height>120mm)

Methods

The overall accuracy was assessed for different combinations of four clip-on with three EH-ACE 7+ Shears and two EH-ACE+ Shears, and evaluated on ease-of-use in clinical practice. The workflow of the experiment consisted of three reoccurring components; clip-on calibration, registration and accuracy measurement. First, the set-up is explained, then the three reoccurring components are explained, followed by the workflow, analysis and statistical analyses.

Set-up

The TTFG cannot measure any data in the first 120 mm from its surface. Therefore, a non-ferromagnetic spacer was placed on top of the TTFG to reach the measurable field. On top of this, both the calibration phantom and pyramid phantom were fixated with tape. Accidental movements of the pyramid phantom were automatically compensated by SurgNav using a Philips 5DOF Patient Sensor fixed on the pyramid. The set-up is visualised in Figure 2.2

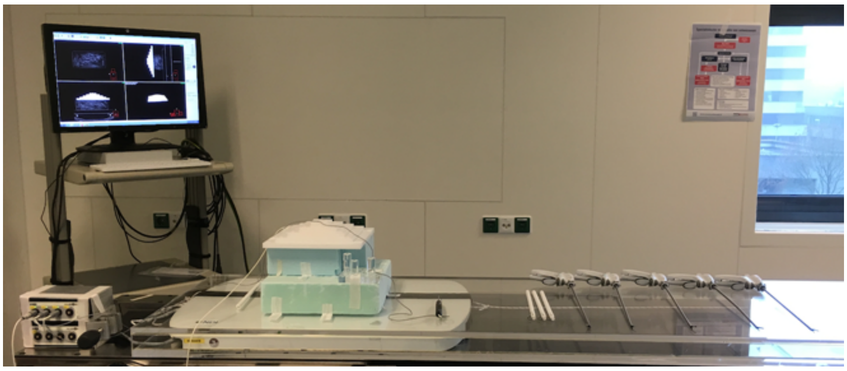

(a) Experiment set-up

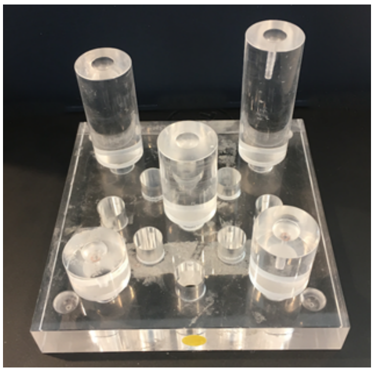

(b) Clip-on calibration phantom

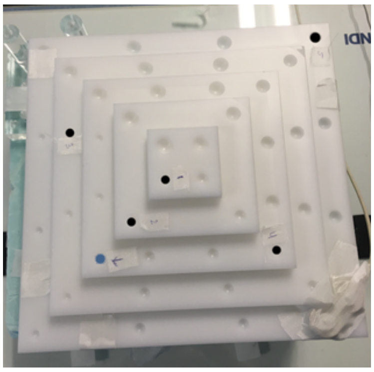

(c) Pyramid phantom

Figure 2.2: The experimental set-up for the calibration of the clip-on (a). The clip-on calibration phantom (b) was used for the clip-on calibration. The five black divots of the pyramid phantom (c) were used for the registration. The accuracy assessment was performed with the dark blue divot (c)

Clip-on calibration: pivoting

The tip of the EH-ACE was placed in the divot of the clip-on calibration phantom and pivoted in a conical shape for 30 seconds with a frame frequency of 40 Hz and an angle of 30 to 60 degrees from the vertical using NDI Architect software. The positions of the Aurora 6DOF Cable Tool were saved during the data acquisition. These positions are located on a sphere, with the tip of the EH-ACE as the origin. NDI Architect software fitted a sphere on these positions, to calculate the tip off set between the Aurora 6DOF Cable Tool and the tip of the EH-ACE. Therefore, it is important to keep the tip as stationary as possible.

Registration from EM-system to CT-system

For the accuracy measurement it was important to link the pyramid phantom expressed in the EM-system to the CT scan of the pyramid phantom. This was done through a point match procedure in SurgNav. The CT scan was loaded into SurgNav and the coordinates of five divots as seen in Figure 2.2c, were determined. The EM coordinates of the corresponding five divots were obtained by placing the Aurora 6DOF Probe in the bottom-centre of those divots. SurgNav automatically calculated the most optimal transformation matrix from EM-system to CT-system, consisting of rotation matrix (${}^{CT}\mathbf{R}_{EM}$) and a translation vector (${}^{CT}\mathbf{t}_{EM}$). The performance of this transformation matrix is expressed as the fiducial registration error (FRE) in RMSE.

Accuracy of the clip-on calibration

One divot of the pyramid phantom was used for the accuracy measurement (Figure 2.2c). The CT coordinates of the divot were determined in SurgNav and stated as reference coordinates. Thereafter, the EM coordinates were obtained by placing the tip of the EH-ACE or the Aurora 6DOF Probe in the bottom-centre of the divot. The position expressed in EM-system (${}^{EM}\mathbf{p}$) was automatically transformed to the position expressed in CT-system (${}^{CT}\mathbf{p}$) with the previous determined rotation matrix (${}^{CT}\mathbf{R}_{EM}$) and translation vector (${}^{CT}\mathbf{t}_{EM}$) in SurgNav, using the following equation:

$$ {}^{CT}\mathbf{p} = {}^{CT}\mathbf{R}_{EM}\, {}^{EM}\mathbf{p} + {}^{CT}\mathbf{t}_{EM} \tag{2.1} $$

The recording of the EM coordinates was repeated six times. The ED (ED) was calculated between the EM coordinates expressed in CT-system (x, y, z) and the reference coordinates $(x_{ref}, y_{ref}, z_{ref})$ for every recording, with the following equation:

$$ ED = \sqrt{(x - x_{ref})^2 + (y - y_{ref})^2 + (z - z_{ref})^2} \tag{2.2} $$

From the six ED ($n = 6$) a single TRE was derived expressed as a RMSE.

$$ RMSE = \sqrt{\frac{\sum_{i=1}^{n} ED_i^2}{n}} \tag{2.3} $$

Workflow
The clip-on tools were named arbitrarily A, B, C, D. The three EH-ACE 7+ Shears were numbered arbitrarily I, II, III and the two EH-ACE+ Shears were numbered arbitrarily IV, V. First, the calibration of clip-on A with EH-ACE I was determined, the registration from EM- to CT-system was performed and the accuracy was determined as previously stated. Thereafter, the same clip-on A was combined with a different EH-ACE (II, III, IV, V). Accuracy measurements were acquired, but without performing a new calibration and registration procedure. The same was done for clip-on B and clip-on D. Last, clip-on C was also combined with EH-ACE I, calibrated, registered and the accuracy measurement was performed. Thereafter, the same calibration and registration was used for the accuracy measurement with all the clip-on (A, B, C, D) and EH-ACE combinations, see Figure 2.3.

Analysis
The final choice for the clip-on calibration to be clinically implemented, depends on the accuracy determined by the TRE and easy of use in clinical practice of the three different clip-on calibrations; individual, pair and generic.

The individual calibration states that a calibration of a clip-on/sensor/EH-ACE combination, can only be used for that specific combination. In this experiment four calibrations took place, the accuracy measurements that directly followed the calibration represent the accuracy of the individual calibration, see the dark blue colour in Figure 2.3.

The pair calibration states that a calibration of each unique clip-on/sensor pair can be used with any EH-ACE. In this experiment the accuracy measurements using the calibrated clip-on with a different EH-ACE represents the accuracy of the pair calibration, see the second lightest colour in Figure 2.3.

The generic calibration states that a calibration of only one clip-on/sensor/EH-ACE combination, can be used with any clip-on and any EH-ACE. In this experiment the accuracy measurements using a different clip-on then the one used for calibration, in combination with any EH-ACE represents the accuracy of the generic calibration, see the lightest blue colour in Figure 2.3.

An outlier analysis with interquartile range (IQR) rule of three was performed on the accuracy of the three different clip-on calibrations [42]. Possible outliers were removed and the measurements of the combinations were the outliers occurred were repeated. The analysis of variance (ANOVA) was performed with IBM SPSS Statistics 25 to analyse if there is a significant difference in those three groups, disregarding the outliers. The outcome was considered significant if the probability value was smaller than 0.05 ($p < 0.05$).

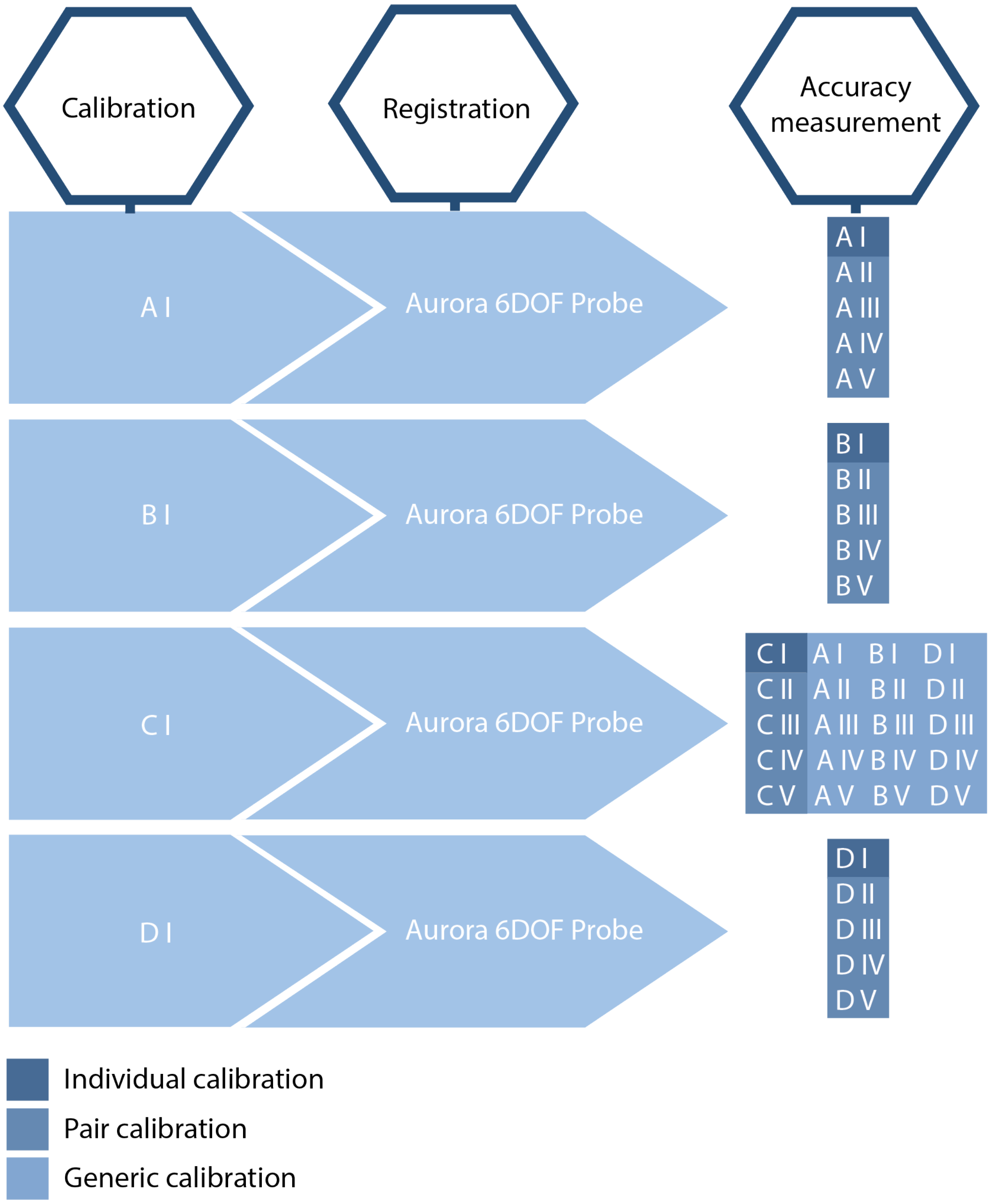

Figure 2.3: Each clip-on was named arbitrarily A-D and each EH-ACE I-V. A clip-on combined with EH-ACE I is calibrated, followed by a registration and an accuracy measurement. Without performing a new calibration or registration the other accuracy measurements are performed with the stated combinations.

2.2.3 Results

The outlier analysis reveals two outliers, using clip-on C in combination with EH-ACE III, with a TRE of 3.7 cm and V with a TRE of 3.8 cm, see Figure 2.4 and Figure 2.5b. The high TRE of the outliers are caused by closely situated ED (Figure 2.4). The outliers were excluded from further analysis.

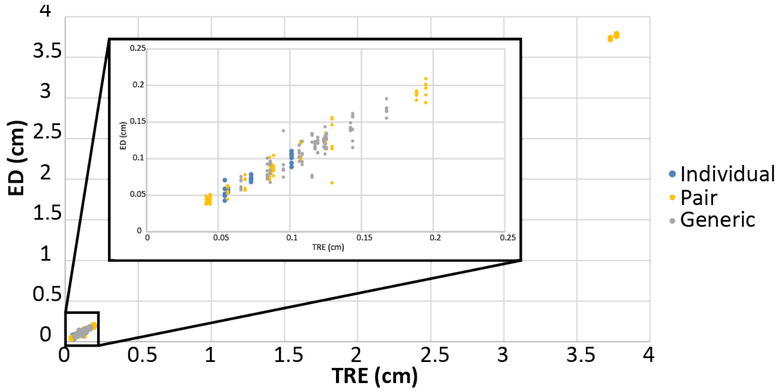

Figure 2.4: Data distribution of the accuracy measurements of the three clip-on calibrations. Where the six repeated ED are plotted against their TRE. The two TRE outliers are visualised in orange at the upper right corner of the graph

The FRE for the four registration were 0.39 mm, 0.49 mm, 0.39 mm and 0.41 mm.

The TRE of the individual calibration stays below the 0.1 cm, see Figure 2.5a. The TRE of the pair calibration and generic calibration stay below the 0.2 cm, see Figure 2.5b and Figure 2.5c. There was no significant difference in the accuracy between the different clip-on calibration options (p=0.193).

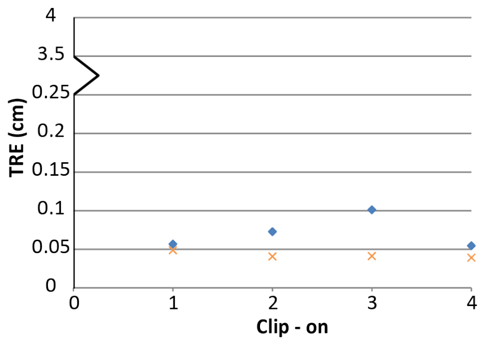

(a) Individual calibration

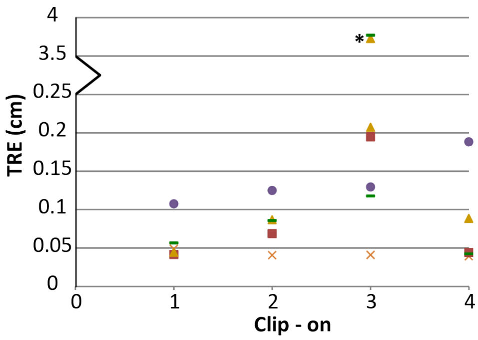

(b) Pair calibration

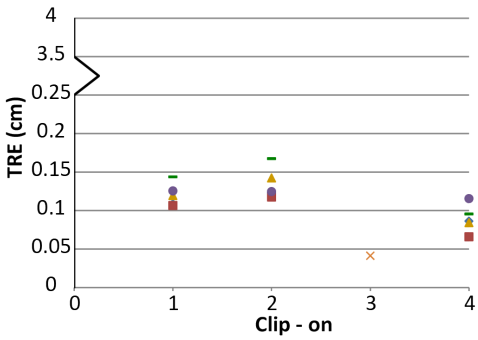

(c) Generic calibration

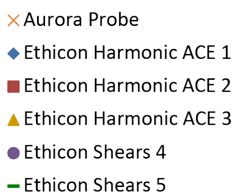

(d)

Figure 2.5: The accuracy of the three different clip-on calibrations. The two TRE outliers are pointed out in Pair calibration (b) with a '*'

2.2.4 Discussion

The aim of the experiment was to determine which clip-on calibration must be used. There are three different clip-on calibrations:

1. Individual calibration.
   Each unique clip-on/sensor/EH-ACE combination is calibrated, which can only be used for the specific set
2. Pair calibration.
   Each unique clip-on/sensor pair is calibrated individually, which can be used with any EH-ACE
3. Generic calibration.
   Only one clip-on/sensor/EH-ACE is calibrated, which can be used with any clip-on and any EH-ACE.

The ED of the outliers are precise, but not accurate, see Figure 2.4. This could mean that the clip-on was not attached correctly to the EH-ACE. After identification of the outliers, the clip-on was reattached to the EH-ACE and accuracy measurements were repeated. The TRE of the repeated accuracy measurements are in line with the other TRE, which strengthen the presumption that incorrect attachment of the clip-on caused the outliers. Further research is necessary in how to prevent the outliers.

Based on the accuracy measurements of this experiment, there is no significant difference between a individual calibration, pair calibration and generic calibration. Generic calibration has the highest ease-of-use in clinical practice, because only a single calibration is required. Therefore, generic calibration will be the most favourable option. However, for the ANOVA, it was assumed that the data is normally distributed and there is a homogeneity of variance. These assumptions were plausible, but difficult to verify due to the small amount of accuracy measurements with the individual calibration.

As explained before, the EH-ACE is a disposable laparoscopic instrument. Therefore, individual calibration requires the calibration to be performed in the sterile environment of the OR, just before the start of the surgical procedure. Pair and generic calibration do not require a sterile environment and can be performed days before the surgical procedure, because the calibrated clip-on can be recombined with another sterile EH-ACE. This prevents additional surgery time. Individual calibration shows to be the most accurate method with a TRE of 0.1 cm compared to pair calibration and generic calibration with a TRE of 0.2 cm. A difference of 0.1 cm between the individual calibration, and the pair and generic calibration is not clinically relevant considering the effort for a calibration in a sterile environment, just before the start of the surgical procedure. Regarding, the ease-of-use of pair and generic calibration; the generic calibration requires a single calibration, while pair calibration needs a calibration for every new clip-on. A new calibration for every clip-on costs time and consequently money. The difference between pair and generic calibration is smaller than 1 mm and not clinically relevant, therefore the preferable method is more dependent on the ease-of-use in clinical practice. So even, if the differences in accuracy between the three different clip-on calibrations would have been significant, the generic calibration remains the most favourable method.

Regarding the two different EH-ACE instruments, the TRE of the EH-ACE+ Shears is slightly higher compared to the EH-ACE 7+ Shears. This might be caused by a differences in dimensions between the instruments. Currently, surgical navigation for colorectal cancer surgery at the NKI-AvL is used as indicator for the location of the tumour area. Therefore, a separate clip-on calibration for the EH-ACE+ Shears is clinically not relevant. However, when surgical navigation will be used as guide to determine the resection margins during laparoscopic colorectal surgery, then a separate clip-on calibration for the EH-ACE+ Shears might be required.

Ideally, there is one registration from EM- to CT-system for all measurements. In that case, the FRE is the same for all accuracy measurements. The registration from EM- to CT-system could not be saved in SurgNav as a result of an error in the software. The software SurgNav and NDI Architect could not run at the same time on a computer. Therefore, every time a clip-on calibration was performed in NDI Architect, the SurgNav software needed to be closed. Consequently, after calibration, a new registration from EM- system to CT-system was needed. The resulting FRE were 0.39 mm, 0.49 mm, 0.39 mm and 0.41 mm. The differences between the FRE are small enough that they will not influence the results in such a way that is clinically relevant.

The clip-on calibration accuracy might improve with a different phantom. Before the start of this experiment it was noticed that the divots of the accuracy phantom are too big for pivoting, see Figure 2.2. The tip of the AH-ACE is free to move in small circular movements inside the divot. Therefore, the calculated tip location will be above the actual tip. Accordingly, it was decided to use the clip-on calibration phantom for the calibration, see Figure 2.2. The divots of the clip-on calibration phantom are too small and too deep. Occasionally, the tip slips out of the divot, causing inaccuracies. A higher clip-on calibration accuracy might be reached with a different phantom. A 3D-printed sphere with a gap might be fabricated, were the tip of the EH-ACE fits perfectly. In turn, the 3D printed sphere would fit perfectly in a divot of the accuracy phantom. The distance between the tip and the bottom-centre of the divot is known, so a pivoting procedure could be performed and the tip location could be calculated.

2.2.5 Conclusion

There was no significant difference between the clip-on calibration methods. The best clip-on calibration method is the generic calibration method where only a single clip-on/sensor/EH-ACE combination is calibrated, which can be used with any clip-on and any EH-ACE with that specific Aurora 6DOF Cable Tool.

2.3 Accuracy in the TTFG workfield

2.3.1 Introduction

The EH-ACE with clip-on will be used to show the location of the EH-ACE in relation to important anatomical structures on pre-operative imaging. Surgical navigation using the clip-on can take place inside the entire TTFG workfield, but the accuracy of the TTFG is not constant over the entire volume [33]. The surgeon needs to know how well EM-tracking with the clip-on performs before clinical implementation. Therefore, it is important to determine the accuracy inside the entire workfield and not only at a single point. The accuracy will be expressed in RMSE. Previous research, shows a RMSE of 1 mm for the laparoscopic pointer [43]. Tracking with the clip-on must come close to this accuracy and preferably <3 mm, to make clinical implementation possible. Besides that, the accuracy must be reproducible.

2.3.2 Materials and Methods

Materials

- Aurora 6DOF Probe (straight tip, standard, NDI 610065)
- Aurora 6DOF Cable Tool (diameter=2.5 mm, length = 2000mm, NDI 610016)
- Ethicon Harmonic ACE 7+ (HARH36, shaft length = 360 mm, diameter=5 mm)
- Clip-on
- Tabletop field generator (V2 System, Northern Digital Inc., Waterloo, Cananda)
- NDI Tool Tracker Software (Northern Digital Inc.)
- Rectangular phantom
- Non-ferromagnetic spacer (height>120mm)
- Matlab (R2018a, The MathWorks, Natick, MA, USA)

Methods

The accuracy in the TTFG workfield is determined by the Aurora 6DOF Probe and EH-ACE 7+ with calibrated clip-on, as described in section 2.2. First, the set-up is explained, followed by the workflow to determine the accuracy inside the entire workfield of the TTFG and the reproducibility of this accuracy with a different Aurora 6DOF Cable Tool, clip-on and EH-ACE.

Set-up

The TTFG cannot measure any data in the first 120 mm from its surface. Therefore, a non-ferromagnetic spacer was placed on top of the TTFG to reach the measurable field. On top of this, the rectangular phantom was fixed. The phantom consisted of four layers. Each layer had seven positions where a rectangular plateau could be inserted. This plateau had four plus-shaped marks, of which the centre was used as point of interest. Consequently, the rectangular phantom consisted of 112 $(n = 4 \cdot 7 \cdot 4 = 112)$ points divided over the entire TTFG workfield. The plus-shaped marks were covered with tape to prevent slipping of the tip of the instrument. The rectangular phantom and set-up are visualised in Figure 2.6.

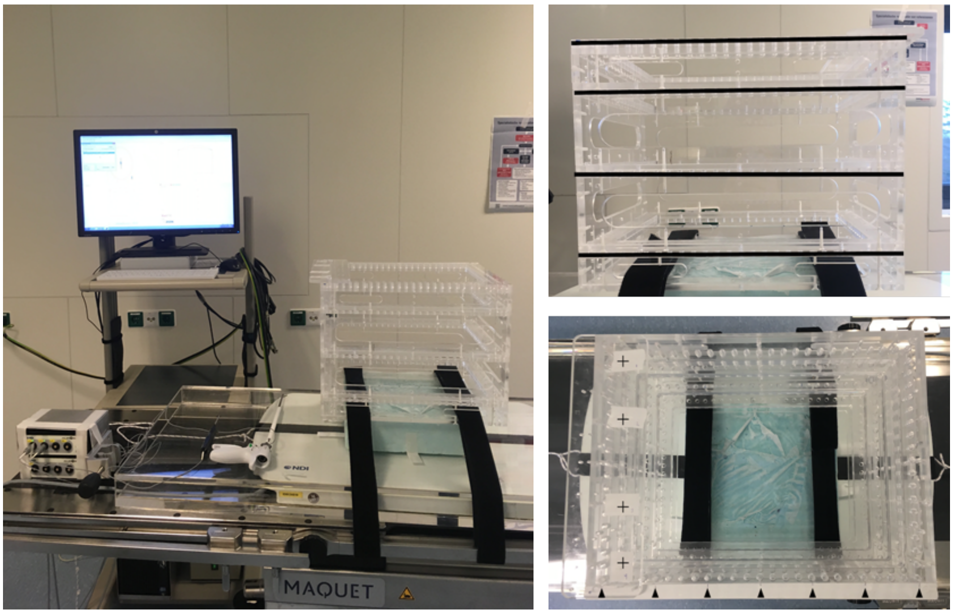

(a) Experiment set-up

(b) Rectangular phantom

Figure 2.6: Experiment set-up (a) for accuracy measurements in the navigated 3D volume. The rectangular phantom (b) with the four layers in the top image and the four plus-shaped marks with the seven positions, pointed out with the triangles, in the bottom image

Workflow

The rectangular plateau was placed on the left side of the bottom layer. First, the Aurora Probe was placed in the centre of the four plus-shaped marks. Thereafter the tip of the EH-ACE 7+ was placed in the four plus shaped marks, before moving the plateau to the next position. Both instruments were hold in a vertical position. For every measurement the tip was kept stationary. 45 data samples ($m = 45$) were obtained in approximately one second by the NDI Tool Tracker software. The average was calculated (Eq. 2.4) to compensate for environmental noise and small hand movements.

$$\overline{\mathbf{p}} = \frac{1}{m} \sum_{i=1}^{m} \mathbf{p}_i \tag{2.4}$$

The Aurora Probe was stated as ground truth for the positions of the points of interests. The ED for every point of interest was calculated between the average position of the Aurora Probe $(x_{ref}, y_{ref}, z_{ref})$ and the EH-ACE 7+ Shears (x, y, z), using Eq. 2.2. An outlier analysis was performed with IBM SPSS Statistics 25 using the ED data. An IQR of three was used to detect possible outliers [42]. Possible outliers were removed from $n = 112$. A RMSE of the entire TTFG workfield is calculated based on these results using Eq. 2.3.

Reproducibility

In order to examine the reproducibility of the accuracy in the entire TTFG workfield, the workflow was repeated with another Aurora 6DOF Cable Tool, clip-on and EH-ACE 7+ Shears, calibrated as described in section 2.2.

An unpaired T-test was performed using the ED without the outliers and IBM SPSS Statistics 25, to determine if there was a significant difference in accuracy of the TTFG workfield. The outcome was considered significant if the probability value was smaller than 0.05 $(p < 0.05)$.

Results

During the experiments two measurement errors occurred where the system failed to measure any data, one in repeat 1 and one in repeat 2. Thereafter, the outlier analysis revealed three outliers in the repeat 1, see Figure 2.7.

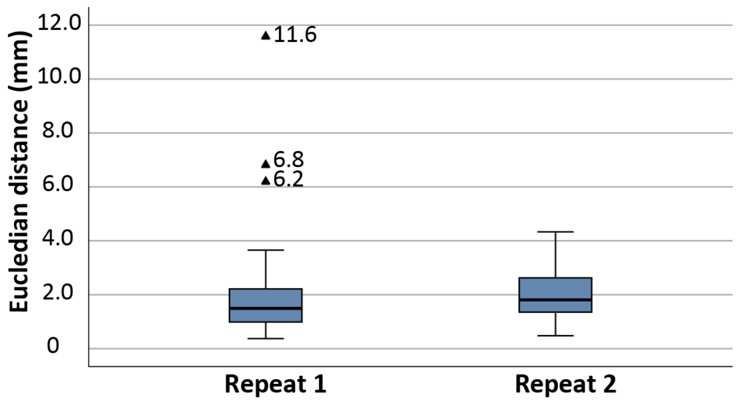

Figure 2.7: Boxplot outlier analysis of the accuracy in the TTFG workfield

The ED without the outliers are visualised in Figure 2.8. The ED of the rectangular phantom top layer are larger compared to the ED of the lower layers of the rectangular phantom. There was a significant difference between ED of repeat 1 versus repeat 2 ($p = 0.004$). Repeat 1 shows a RMSE of 2.2 mm and the repeat 2 shows a RMSE of 2.4 mm.

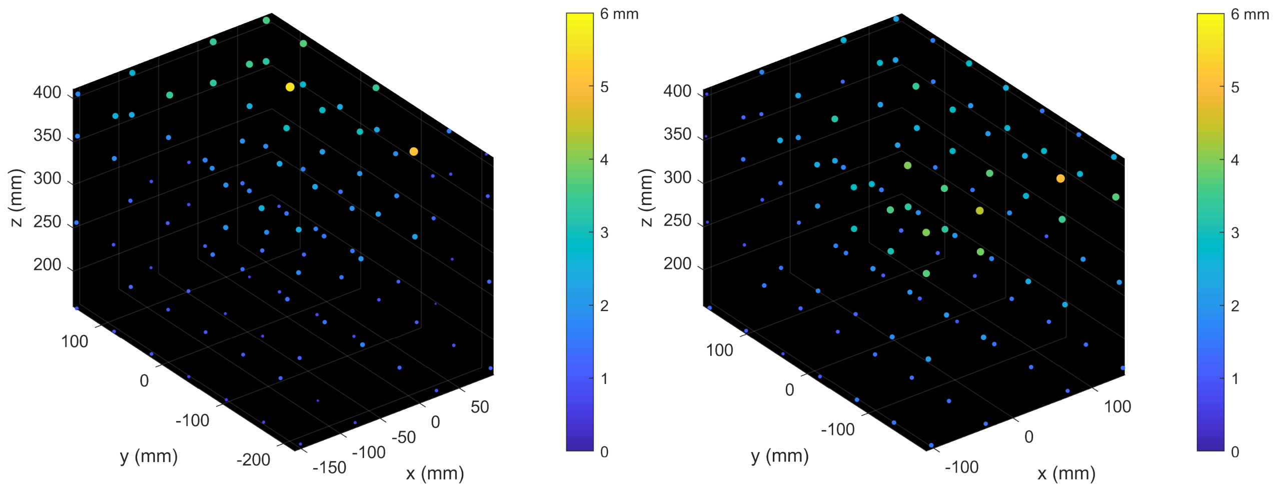

(a) Euclidean distances of repeat 1

(b) Euclidean distances of repeat 2

Figure 2.8: Euclidean distances of the TTFG workfield

2.3.3 Discussion

The aim of the experiment was to determine the accuracy of tracking with the clip-on and EH-ACE inside the workfield of the TTFG.

The two detected measurement errors are caused by a broken wire inside the Aurora 6DOF Probe. The NDI Tool Tracker software announced 'broken sensor' a couple of times for the Aurora 6DOF Probe. In these cases the data samples were repeated. Unfortunately, two times the announcement did not occur, causing the measurements errors in the data. The detected outliers occurred at the top layers of the rectangular phantom. The Aurora 6DOF Cable Tool of the clip-on balanced on the edge of the workfield of the TTFG, a slight movement caused the NDI Tool Tracker announcement, 'sensor partly out of volume'. This might caused the outliers on the top layer of the rectangular phantom.

The observed significant difference of 0.2 mm between repeat 1 and repeat 2 ($p = 0.004$) is not considered clinically relevant. Therefore, tracking with another Aurora 6DOF Cable tool is possible with an accuracy of approximately 2 mm for the entire workfield.

Previous research evaluated the accuracy of the laparoscopic pointer and revealed a RMSE of approximately 1 mm [43]. The clip-on shows a higher RMSE value of 2.4 mm. However, these measurements cannot be compared since they were not determined in the same way. With increasing distance from the TTFG, the accuracy decreases [33]. The rectangular phantom contains 112 points of interest, and covers almost the entire TTFG workfield, also the parts that are less accurate. The phantom used in the laparoscopic pointer experiment is much smaller, only cover the bottom-centre of the TTFG workfield, and had only four points of interest that were evaluated [43]. In order to make a fair comparison, the measurements of the laparoscopic pointer should be repeated using the rectangular phantom and the above explained workflow. Nevertheless, surgeons in the NKI-AvL prefer surgical navigation with the clip-on rather than the laparoscopic pointer, when the difference in accuracy is 1 mm.

The ED of the top layer of the rectangular phantom are larger compared to the bottom layer. The EM tracking accuracy with clip-on is more accurate at the bottom of the workfield closer to the TTFG, compared to the top of the workfield. These results are similar to those reported in another study [33]. For the most accurate tracking it is advised that the tip of the EH-ACE stays in the first 30 cm of the TTFG workfield.

There was a systematic error in the z-direction. The z-coordinates of the Aurora 6DOF Probe, was further from the TTFG than the z-coordinates of the clip-on with EH-ACE. It is possible that the clip-on during calibration was placed differently, which might cause the systematic error. Another possibility might be movement of the rectangular plateau. When the tip was placed in a point of interest, the plateau rotated a little bit downwards, especially at the right side of the rectangular phantom were there was less support from the phantom. The clip-on with EH-ACE is heavier compared to the Aurora 6DOF Probe. Therefore, the plateau might rotate more with the EH-ACE compared to the Aurora 6DOF Probe. This might also explain the higher ED at the right side of the rectangular phantom. The rectangular phantom was not perfectly level, and had a small slope regarding to the TTFG. As mentioned earlier, with an increasing distance to the TTFG, the accuracy decreases [33]. Another explanation for the bigger ED at the right side might be that this slope caused the bigger ED.

To have an accurate comparison, the tip of the Aurora 6DOF Probe and the tip of the EH-ACE with clip-on need to be placed at the exact same location. Unfortunately, this was pretty hard, because the point of interest was the centre of a plus-shaped mark wherein the tip could move minimally. For the future a phantom which covers the entire TTFG workfield with divots specifically designed for the tips would be preferable. In this way, you have a bigger chance of placing the tips in exact the same location.

The Aurora 6DOF Probe is stated as ground truth. However, the calibration of the Aurora 6DOF Probe might also have inaccuracies, which are included in the accuracy of tracking with the clip-on.

2.3.4 Conclusion

The tracking accuracy of the clip-on with EH-ACE inside the entire TTFG workfield is 2 mm. When another Aurora 6DOF Cable Tool was used, a significant difference of 0.2 mm was observed in the RMSE, which was not deemed clinical relevant.

2.4 Accuracy during ultrasonic diathermy

2.4.1 Introduction

As explained earlier, ultrasonic technology transforms electrical energy to mechanical energy in the form of vibrations. It is still unknown if this electrical energy might interfere with the EM tracking. Interference is most likely to occur during activation.

2.4.2 Materials and Method

Materials

- Tabletop Field Generator (V2 System, Northern Digital Inc., Waterloo, Cananda)
- Aurora 6DOF Cable Tool (diameter=2.5 mm, length = 2000mm, NDI 610016)
- Software NDI Tool Tracker (Northern Digital Inc.)
- Ethicon Harmonic ACE 7+ (HARH36, shaft length = 360 mm, diameter=5 mm)
- Clip-on
- Chicken breast
- Ethicon Harmonic Gen11 Endo-surgery Generator (GEN11)
- Harmonic Hand Piece (HP054)
- Matlab (R2018a, The MathWorks, Natick, MA, USA)

Methods

Set-up

The EH-ACE 7+ was connected to the Ethicon Harmonic G11 Endo-surgery Generator (G11 Endo-surgery) using the Harmonic Hand Piece. The minimal power level of the G11 Endo-surgery was set on the default value 3 and the maximum power level on 5 [44]. The Aurora 6DOF Cable Tool was attached to the EH-ACE 7+, approximately 12 cm from the tip. The tip-offset between the Aurora 6DOF Cable tool and the tip of the EH-ACE 7+ was determined following the clip-on calibration, as described in section 2.2. Chicken breast will be used during this experiment, to simulate tissue being coagulated. To prevent contamination of the EM sensor with chicken breast, an US sleeve was placed over the EM sensor and the Harmonic Hand Piece and sealed with tape. The EH-ACE 7+ with Aurora 6DOF Cable Tool was fixated on top of a cardboard box inside the TTFG workfield. The whole set-up was placed in a fume hood, for possible smoke and stench formation (2.9 for the set-up).

Figure 2.9: Experiment set-up for accuracy measurements during ultrasonic diathermy

Workflow

The influence of the three different vessel sealing buttons; minimal, maximal and advanced hemostasis, were tested. A new piece of chicken breast ($30 \cdot 30 \cdot 10\ mm$) was placed in the tip of the EH-ACE 7+ Shears by applying manual pressure to the handle. For each activation, the position of the tip was recorded with a total data collection time of 30 seconds and a frequency of 40 Hz using NDI Tool Tracker. Consequently, 1200 positions ($m = 1200$) were recorded for each activation. Five seconds after the start of recording, the vessel sealing button was pressed for 3 seconds. This was repeated six times for the three vessels sealing buttons. Thereafter, the activation time was increased from three to ten seconds. The data was collected from the three vessel sealing buttons with a repetition of six times. Last, the EH-ACE 7+ Shears was detached from the G11 Endo-surgery and all data was collected again, this time outside the fume hood and without the actual activation and tip heating. Continuous pressure was applied during the data collection and after every data collection a new piece of chicken breast was placed in the tip.

For every activation, the first 50 ($m = 50$) recorded positions were used to calculate the starting position, using Eq. 2.4. The ED was calculated between the starting position ($x_{red}, y_{ref}, z_{ref}$) and all 1200 saved positions (x, y, z), using Eq. 2.2. For each activation, the recorded positions and calculated ED were analysed over time, to determine if there was a deviation from the starting position during and/or after activation of the EH-ACE 7+ Shears, the extent of the deviation and if this is time based.

2.4.3 Results

The results of pressing the minimal activation button, when the EH-ACE 7+ Shears was connected with the G11 Endo-surgery and placed in the fume hood, are shown in Figure 2.10. The ED increase over time. The coordinates in the x- and z-direction deviate from the starting position, while the y-coordinates remain stable. See Figure 1.3 for the directions of the x-,y-,z-coordinates in the workfield of the TTFG.

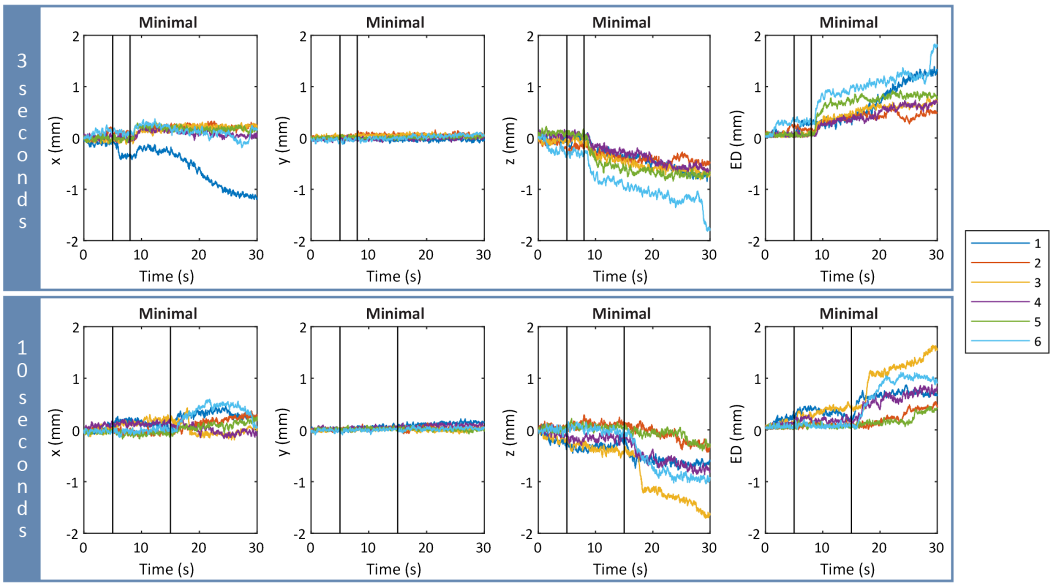

Figure 2.10: The x-, y- and z-coordinates and Euclidean distances over time after minimal activation for three and ten seconds of the EH-ACE 7+ Shears inside the fume hood

The trend visualised in Figure 2.10 concerning the x-, y-, z-coordinates is also observed with pressing the maximal and advanced hemostasis button, when the EH-ACE 7+ Shears was connected to the G11 Endo-surgery and placed inside the fume hood. The increasing ED over time are visualised in Figure 2.11 for all the three vessel sealing buttons.

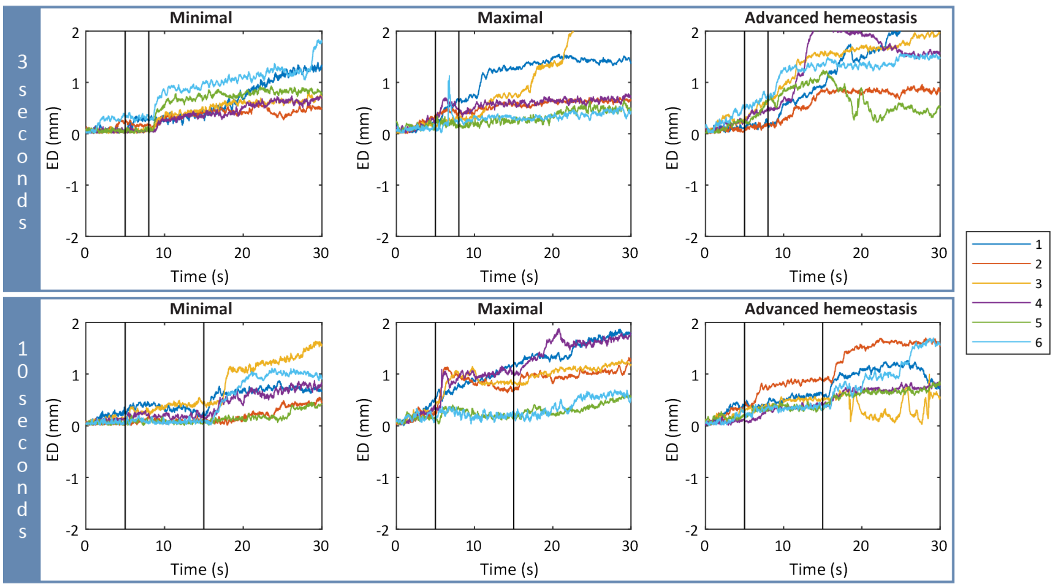

Figure 2.11: Euclidean distance over time after activation of the three vessel sealing buttons for three and ten seconds of the EH-ACE 7+ Shears inside the fume hood.

The ED increases over time, due to a deviating x-coordinate. The y- and z-coordinate remain stable, when pressing the minimal activation button, while the EH-ACE 7+ Shears was detached from the G11 Endo-surgery and placed outside the fume hood, see Figure 2.12.

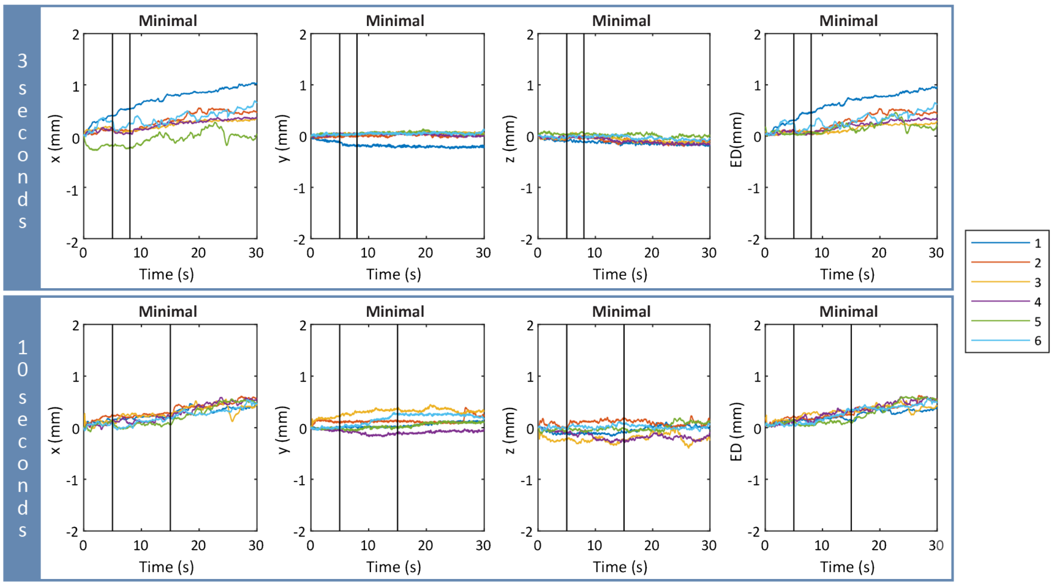

Figure 2.12: The x-, y- and z-coordinates and Euclidean distance over time after pressing the minimal activation button for three and ten seconds outside the fume hood, without actual activation of the EH-ACE 7+ Shears.

The trend visualised in Figure 2.12 concerning the x-, y-, z-coordinates is also observed with pressing the maximal and advanced hemostasis button, when the EH-ACE 7+ Shears was detached from the G11 Endo-surgery and placed outside the fume hood. The increasing ED are visualised in Figure 2.13 for all the three vessel sealing buttons.

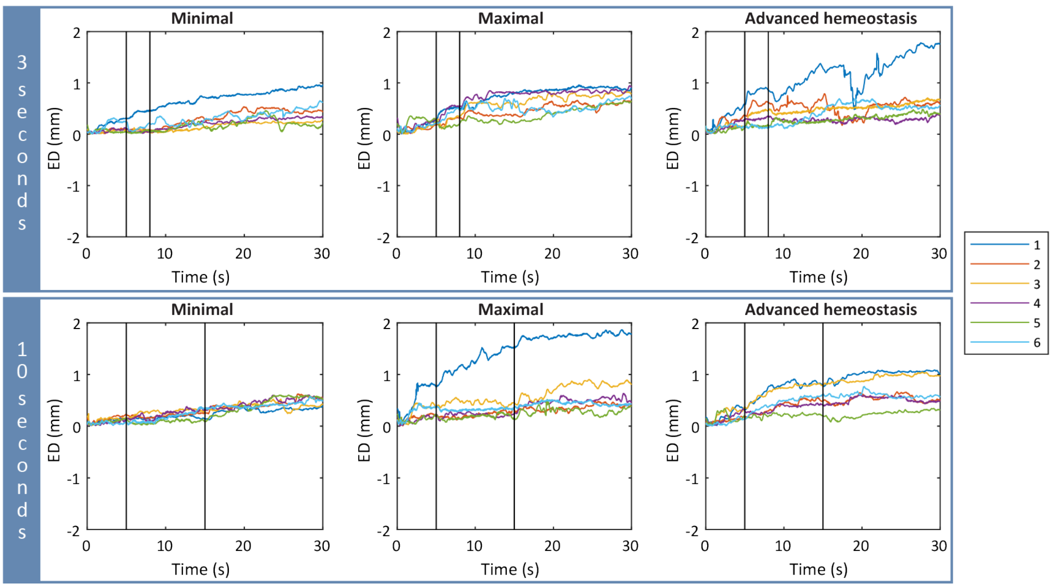

Figure 2.13: Euclidean distance over time, after pressing the three vessel sealing buttons for three and ten seconds outside the fume hood, without actual activation of the EH-ACE 7+ Shears.

The results of pressing no button, when the EH-ACE 7+ Shears was detached from the G11 Endo-surgery and placed outside the fume hood, are visualised in Figure 2.14. The coordinates in the x-, y-, z-direction and the ED remain stable around the starting position.

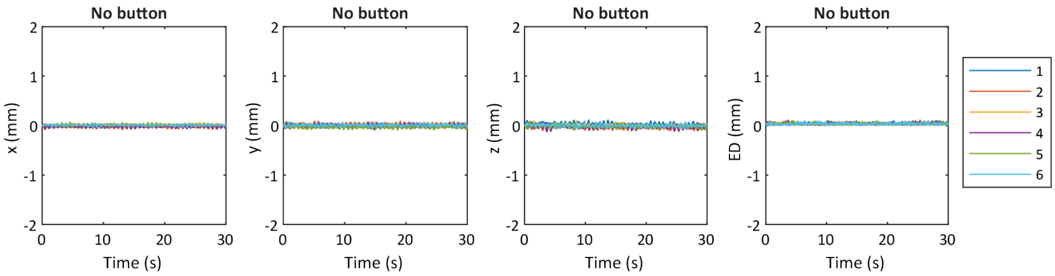

Figure 2.14: The x-, y- and z-coordinates and Euclidean distance over time without pressing the vessel sealing buttons.

2.4.4 Discussion

The aim of the experiment was to determine if activation of the EH-ACE 7+ Shears influences the accuracy of tracking with the clip-on. If disturbances occur, they were expected to occur in the x-, y- and z-coordinates during and directly after the activation of the EH-ACE 7+ Shears. Figure 2.10 shows an increase in ED over time, caused by a deviation from the starting position in the x- and z-direction. However, the y-coordinate remains stable around the starting position. Therefore, it is unlikely that the deviation in the x- and z-direction is caused by the activation of the EH-ACE 7+ Shears. Possible other causes might include; movement of the cardboard box, hand movements, movement of the tip due to coagulation of the chicken breast or a combination of these possibilities. Pressing one of the three vessel sealing buttons might have caused direct movement of the tip or movement of the cardboard box and thereby movement of the tip. During the activation of the EH-ACE 7+ Shears the chicken breast is coagulated, thus decreasing its thickness which might have caused movement of the tip. Furthermore, during the activation of the EH-ACE 7+ Shears the chicken breast sometimes fell from the EH-ACE's grasp as result of the coagulation, which also might have caused movement of the tip. Figure 2.12 shows an increase in ED, only caused by a deviation in the x-direction. However, the z-coordinate remains around the starting position. During these measurements the EH-ACE 7+ Shears was detached from the G11 Endo-surgery, so there was no activation while the buttons were pressed. Consequently, the chicken breast was not coagulated and did not fall down. This might exemplify that the coagulation of the chicken breast caused movements in the z-direction visualised in Figure 2.10. The three vessel sealing buttons were still pressed, which might clarify the deviation in the x-direction from the starting position in Figures 2.10 and 2.12. As a final check, the measurements were repeated while no button was pressed, see Figure 2.14. The x-, y-, z-coordinates and ED remain around the starting position. This strengthens the explanation that the hand movements caused the deviation in the x-direction from the starting position, visualised in Figure 2.10 and Figure 2.12.

During the measurements it was noticed that the tip is really hot, but the shaft of the EH-ACE 7+ Shears does not heat up during the three and ten second activation. This is also stated by the manufacturer of the EH-ACE 7+ Shears [45]. Therefore, it is most likely that the clip-on will not deform due to activation of the EH-ACE 7+ Shears.

The EH-ACE+ Shears uses the same ultrasonic technology. The only difference are the vessel sealing buttons (Figure 1.7). The EH-ACE 7+ Shears has minimal, maximal and advanced hemostasis, while the EH-ACE+ Shears has only minimal and maximal vessel sealing buttons. Concluding, the results of this experiment could be extended to the EH-ACE+ Shears.

If this experiment will be repeated in the future, it is advised to use a non-metal bench vice instead of the cardboard box. The disturbances due to the activation of the EH-ACE 7+ Shears were smaller, than expected. Therefore, the stability of the set-up has a bigger influence on the outcome. A non-metal bench vice would be less prone to movement disturbances compared to the cardboard box.

The activation time of the EH-ACE 7+ Shears is limited by the coagulation time of the chicken breast. The ten seconds activation of the EH-ACE 7+ Shears was the limit, otherwise the EH-ACE 7+ Shears would become unusable through damage. If analysis of longer activation time is preferred, another way of heat release must be used.

The results of this experiment only apply to diathermy with ultrasonic technology. If EM tracking will be used in combination with a monopolar or bipolar diathermy instrument, a new examination must be done to asses the influence of those instruments on the EM tracking accuracy. It might be possible that the monopolar or bipolar diathermy instruments cause bigger inaccuracies compared to an ultrasonic instrument. Monopolar and bipolar instruments have electrical energy in the shaft and a current between the electrodes [34]. The Hand Piece of the EH-ACE converts the electrical energy to mechanical energy [46]. There is no electrical energy in the patient, or close to the Aurora 6DOF Cable Tool and TTFG workfield. Therefore, it might be possible that the monopolar or bipolar diathermy instruments cause bigger inaccuracies compared to a ultrasonic diathermy instrument.

2.4.5 Conclusion

The activation of the minimal, maximal and advanced hemostasis vessel sealing buttons of the EH-ACE 7+ Shears does not seem to influence the accuracy of tracking with the clip-on. Surgical navigation can also be used during activation of the EH-ACE.

3 Registration with 3D tracked ultrasound for abdominal surgical navigation

3.1 Introduction

The current CBCT registration for surgical navigation at the NKI-AvL, makes surgical navigation limited available. This method requires a hybrid OR with a CBCT, limiting the number of hospitals able to use surgical navigation. Furthermore, the patient and medical personal are exposed to radiation. There is a high demand for an alternative registration method.

In this phantom study, the accuracy of surgical navigation using tracked 3D US registration will be evaluated. The current registration method using CBCT, is defined as gold standard at the NKI-AvL. The TRE of surgical navigation using CBCT registration is 4.0 mm in a clinical setting [38]. Results in a clinical setting with a patient might differ from a phantom study. Therefore, the TRE of both registration methods, 3D tracked US as well as CBCT, will be determined for a fair comparison.

3.2 Materials and Methods

3.2.1 Materials

- Fake hip bones
- 28 x 28 x 28 plastic box
- 2.2 kg Gelatin powder
- 12 L hot water
- 720 mL alcohol
- 5 Aurora Micro 6DOF Sensors (610059, Northern Digital Inc., Waterloo, Canada)
- 3 Philips Patient Sensors

- Tabletop field generator (V2 System, Northern Digital Inc., Waterloo, Cananda)
- CT scanner (Toshiba Aquilion)
- CBCT (Philips Allura FD20 XperCT)
- CustusX software (version: 18.04, SINTEF, Trondheim, Norway)
- BK medical US system (bk5000, BK Medical, Peabody, MA, USA)
- T-shaped intraoperative transducer (I14C5T, BK Medical, Peabody, MA, USA) with clasp and 6DOF Cable Tool
- 3D Slicer (version: 4.10.1, research platform for analysis and visualisation of medical images)
- Matlab (version: R2018a, The MathWorks, Natick, MA, USA)

3.2.2 Methods

Phantom

Artificial hip bones were placed inside a plastic box (28 x 28 x 28 cm) together with five Aurora Micro 6DOF Sensors positioned at specific locations. Three sensors were placed at the anterior side and two more posterior of the pelvic area. 2.2 kg Gelatin mixed with 740 mL alcohol and 12 L water was added. Care was being taken to avoid air bubbles as much as possible. The phantom was kept at 4 °C to solidify for 24 hours. Subsequently, a CT scan of the phantom was made with a slice thickness of 0.6 mm and a pixel spacing of 0.66 mm. From CT, a 3D model of the phantom was created with a semi-automatic intensity-based segmentation of the bones and the Aurora Micro 6DOF Sensors using 3D Slicer.

Set-up

The TTFG was placed inside the special designed carbon surgical table. The three Philips 5DOF Patient Sensors were attached to the phantom. Thereafter, the phantom was placed on top of a non-ferromagnetic spacer inside the TTFG workfield, see Figure 3.1

Reference points

The five Aurora 6DOF Sensors inside the phantom were used to asses the performance of the CBCT registration and the 3D tracked US registration for surgical navigation. After registration the positions of the Aurora 6DOF Sensors expressed in EM-system were transformed to CT-system. The difference between the transformed positions and the actual positions expressed in CT-system were used to calculated the TRE after registration.

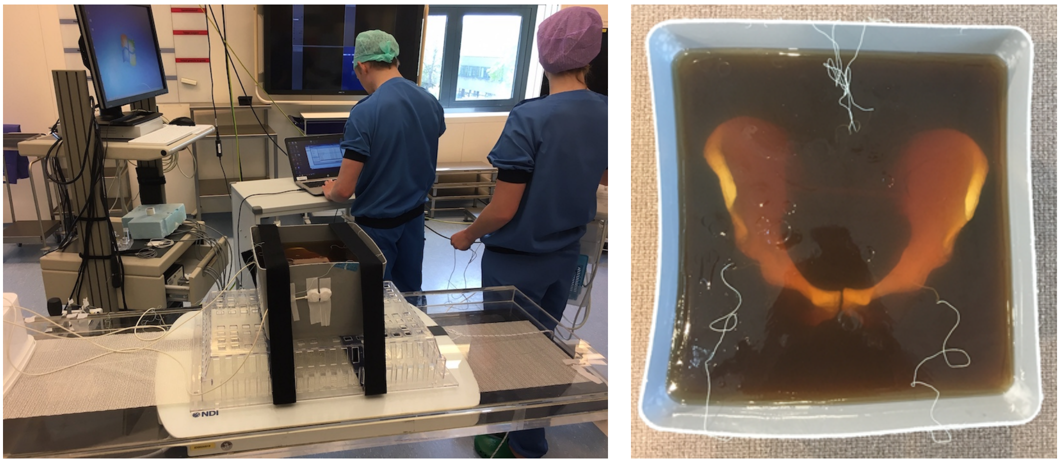

(a) Experiment set-up **(b)** The phantom with artificial hip bones

Figure 3.1: Experiment set-up (a) to evaluate the accuracy of surgical navigation using 3D tracked US registration with a phantom (b).

The actual position of the five Aurora Micro 6DOF Sensors ($k = 1, ..., 5$) were determined six times (m = 6) in the CT scan of the phantom. The mean position of every Aurora Micro 6DOF Sensor expressed in CT-system was calculated (${}^{CT}\overline{\mathbf{p}}_k$), using Eq. 3.1.

$$ {}^{CT}\overline{\mathbf{p}}_k = \frac{1}{m}\sum_{i=1}^{m} {}^{CT}\mathbf{p}_{k,i} \tag{3.1} $$

CBCT protocol

As explained in section 1.2.4, two registrations are needed when using the CBCT; CBCT-system to CT-system and from EM-system to CBCT-system. A schematic overview of the coordinate systems is visualised in Figure 1.9. The Philips 5DOF Patient Sensors were used for the registration and the Aurora Micro 6DOF Sensors as reference points to determine the TRE.

First, the positions of the five Aurora Micro 6DOF Sensors expressed in EM-system were saved (40 samples/position). A CBCT scan of the Philips 5DOF Patient Sensors was needed for the registration. The field of view of the CBCT was too small to image all the Philips 5DOF Patient Sensors in a single scan. Therefore, two CBCT scans were made (Philips Allura FD20 XperCT) with a slice thickness of 0.66 mm and a pixel spacing of 0.66 mm. The positions of the five Aurora Micro 6DOF Sensors expressed in EM-system were saved again (40 samples/position) to determine if there was any movement resulting from the CBCT scans. For the registration from CBCT-system to CT-system, the CT scan and the CBCT scans were loaded in the SurgNav software. A pre-matching was performed based on the centre of mass of both scans. Thereafter, manual adjustments could be made by translation and rotation of the CBCT imaging in the transverse, sagittal and coronal view. When an adequate overlap between the CT and CBCT imaging was achieved, the bone-bone registration of SurgNav was executed to determine the transformation matrix (${}^{CT}\mathbf{T}_{CBCT}$). The result of the registration was visually checked with the green/purple mode that highlights differences between the CT- and the CBCT imaging and the cut mode were it could be checked if the bone contours overlap.

Second, the Philips 5DOF Patient Sensors were used for the registration from EM-system to CBCT-system. The Philips 5DOF Patient Sensor actually consists of two 5DOF EM-Sensors, therefore the three Philips 5DOF Patient Sensors have six EM-sensors. The six positions ($n = 6$) of the EM-sensors were semi-automatically determined in the CBCT imaging (${}^{CBCT}\mathbf{q}_\ell$ with $\ell = 1, ..., 6$) . A point-match registration between the positions expressed in CBCT and expressed in EM-system (${}^{EM}\mathbf{q}_\ell$) was performed in SurgNav using the Procrustes algorithm. The centroids of the data set were calculated, see Eq. 3.2.

$$ {}^{CBCT}\overline{\mathbf{q}} = \frac{1}{n}\sum_{i=1}^{n} {}^{CBCT}\mathbf{q}_i \tag{3.2a} $$

$$ {}^{EM}\overline{\mathbf{q}} = \frac{1}{n}\sum_{i=1}^{n} {}^{EM}\mathbf{q}_i \tag{3.2b} $$

To get rid of the translation influence, normalise by subtracting the centroids from all positions, see Eq. 3.3

$$ {}^{CBCT}\breve{\mathbf{q}}_\ell = {}^{CBCT}\mathbf{q}_\ell - {}^{CBCT}\overline{\mathbf{q}} \tag{3.3a} $$

$$ {}^{EM}\breve{\mathbf{q}}_\ell = {}^{EM}\mathbf{q}_\ell - {}^{EM}\overline{\mathbf{q}} \tag{3.3b} $$

The rotation matrix (${}^{CBCT}R_{EM}$) was determined, using Kabsch algorithm. The input consists of the ${}^{CBCT}\breve{\mathbf{q}}_\ell$ and ${}^{EM}\breve{\mathbf{q}}_\ell$ data points in $3 \times n$ matrices $\breve{\mathbf{A}}$ and $\breve{\mathbf{B}}$ The value of $\mathbf{U}$, $\mathbf{S}$ an $\mathbf{V}$ were calculated, such that:

$$ \mathbf{USV}^T = \breve{\mathbf{A}}\breve{\mathbf{B}}^T \tag{3.4} $$

$$^{CBCT}\hat{\mathbf{R}}_{EM} = \mathbf{U}\mathbf{V}^T \tag{3.5}$$

The translation was calculated, using the following equation:

$$^{CBCT}\hat{\mathbf{t}}_{EM} = ^{CBCT} \overline{\mathbf{q}} - ^{CBCT} \hat{\mathbf{R}}_{EM} {}^{EM}\overline{\mathbf{q}} \tag{3.6}$$

The rotation matrix and translation vector were saved in a transformation matrix ($^{CBCT}\mathbf{T}_{EM}$) by SurgNav. SurgNav automatically calculated the transformation matrix ($^{CT}\mathbf{T}_{EM}$) and saved this into a file using Eq. 3.7

$$^{CT}\mathbf{T}_{EM} = ^{CT} \mathbf{T}_{CBCT} {}^{CBCT}\mathbf{T}_{EM} \tag{3.7}$$

A paired T-test was performed with IBM SPSS Statistics 25 on the positions of the five Aurora Micro 6DOF Sensors expressed in EM-system saved before and after the CBCT. Depended on the outcome, one of the data sets will be used for further analysis.

The position of every Aurora Micro 6DOF Sensor expressed in EM-system was saved 40 times ($n = 40$). The mean position of every Aurora Micro 6DOF Sensor ($^{EM}\overline{\mathbf{p}}_k$) was calculated using the following formula:

$$^{EM}\overline{\mathbf{p}}_k = \frac{1}{n}\sum_{i=1}^{n} \mathbf{p}_{k,i} \tag{3.8}$$

The transformation matrix ($^{CT}\mathbf{T}_{EM}$) was extracted from file and multiplied with the position of every Aurora Micro 6DOF Sensor expressed in EM-system ($^{EM}\overline{\mathbf{p}}_k$), in order to express the position in CT-system ($^{CT}\hat{\mathbf{p}}_k$), see equation:

$$^{CT}\hat{\mathbf{p}}_k = ^{CT} \mathbf{T}_{EM} {}^{EM}\overline{\mathbf{p}}_k \tag{3.9}$$

The ED between the transformed positions expressed in CT-system by means of CBCT registration ($^{CT}\hat{\mathbf{p}}_k$ consisting of $^{CT}\hat{x}_k, ^{CT}\hat{y}_k, ^{CT}\hat{z}_k$), and the actual positions

(${}^{CT}\overline{\mathbf{p}}_k$ consisting of ${}^{CT}\overline{x}_k, {}^{CT}\overline{y}_k, {}^{CT}\overline{z}_k$), was calculated for the five Aurora Micro 6DOF Sensors, using Eq. 3.10.

$$ED_k = \sqrt{({}^{CT}\hat{x}_k - {}^{CT}\overline{x}_k)^2 + ({}^{CT}\hat{y}_k - {}^{CT}\overline{y}_k)^2 + ({}^{CT}\hat{z}_k - {}^{CT}\overline{z}_k)^2} \quad (3.10)$$

Thereafter, the TRE expressed as RMSE was calculated, using these five ED with the following formula:

$$RMSE = \sqrt{\frac{\sum_{i=1}^{5} ED_i^2}{5}} \quad (3.11)$$

This CBCT protocol was repeated two more times.

3D tracked US protocol

A schematic overview of the coordinates systems of different components during 3D tracked US registration are visualised in Figure 3.2. The 2D US images and 3D US volume are expressed in the EM-system, due to the calibration of the T-shaped intraoperative transducer with clasp and Aurora 6DOF Cable Tool. Therefore, the 3D US volume (Figure 1.10c) with therein the pelvic bones are expressed in EM-system. Consequently, only one bone-bone registration is needed to determine the transformation matrix (${}^{CT}\mathbf{T}_{EM}$) for surgical navigation using 3D tracked US, compared to the two registration for surgical navigation using CBCT, see Figure 3.2 and Figure 1.9.

First, the positions of the five Aurora Micro 6DOF Sensors (${}^{EM}\mathbf{p}_k$ with $k = 1, ..., 5$) expressed in EM-system were saved (40 samples/position). The B-mode was selected on the BK Medical US system (BK Medical, Peabody, MA, USA, settings; focus: 0-5cm, gain: 3.0, dynamic range: 55dB, B frequency: 1.5 MHz, ETD: 3, ACI: on). The following four sweeps were made with the T-shaped intraoperative transducer (I14C5T) with clasp and Aurora 6DOF Cable Tool using CustusX software:

- Left ilium with iliac crest
- Right ilium with iliac crest
- Os Pubis
- U turn, where in one sweep left ilium, right ilium and os pubis was imaged.

The position and orientation of the 2D US images were saved by CustusX with a sample rate of of approximately 20 frames/s. For every sweep, a 3D US volume

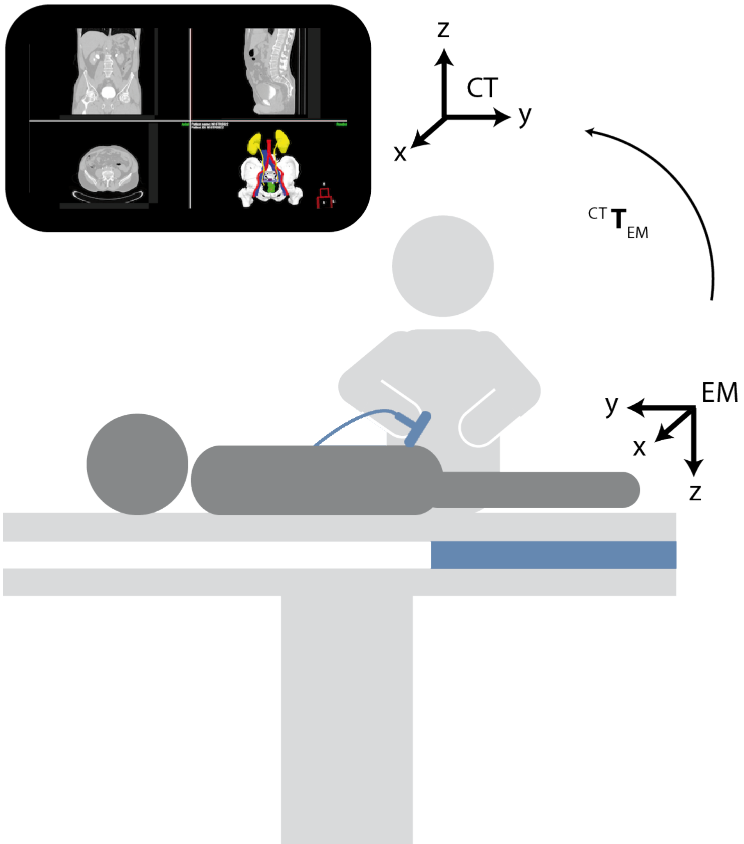

Figure 3.2: Schematic overview of the coordinates systems from different components during surgical navigation using 3D tracked US registration

was automatically created using CustusX, where the 2D images were stacked and interpolated.

The bones from the four sweeps and the pelvic bones from the CT scan were segmented using 3D Slicer (version 4.10.1). From the four sweeps the following combinations were made:

- Left (ilium + iliac crest)
- Left (ilium + iliac crest) + right (ilium + iliac crest)
- Left (ilium + iliac crest) + right (ilium + iliac crest) + os pubis
- Left (iliac crest)
- Left (iliac crest) + right (iliac crest)
- Left (iliac crest) + right (iliac crest) + os pubis
- U-turn

The segmentations of the US weeps and the CT scan consists of 3D points called vertices and the interconnected planes called faces. These vertices and faces together, form a patch. To reduce computation time, these patches were first reduced in size while maintaining the overall shape. The initial transformation was performed by overlaying the centre of mass, using the vertices as point cloud. Thereafter, an Iterative Closest Point algorithm was initialised to overlay the point clouds as best as possible. The point cloud of the US sweeps were stated as the 'moving' point cloud (X), while the the pelvic bones segmentation from CT were stated as 'fixed' point cloud (Y). The input data consisted of $X = \{x_m | m = 1, \cdots, M\}$ and $Y = \{y | n = 1 \cdots N\}$. First, for every point in $\mathbf{y}$ the corresponding point in $\mathbf{x}$ is found were the ED was smallest, using equation:

$$m(n) = argmin||\mathbf{x}_m - \mathbf{y}_n|| \qquad \text{for } m = 1 \cdots M \tag{3.12}$$

The Kabsch algorithm was applied to the found corresponding points, resulting in the rotation matrix $\mathbf{R}$ and translation vector $\mathbf{t}$. All points in X are transformed according to the following equation:

$$\mathbf{x}_m = \mathbf{R}\mathbf{x}_m + \mathbf{t} \tag{3.13}$$

Eq. 3.12 and Eq. 3.13 were repeated until the maximum amount of iterations was reached or the change between two iterative translation vectors and rotation matrices was smaller than a predefined threshold. For this experiment the maximum number of iterations was 300, the threshold for the translation was 0.01 mm and for the rotation 0.009 radians. The final rotation matrix and translation vector were saved into the transformation matrix ${}^{CT}\mathbf{T}_{EM}$, see Figure 3.2.

The positions of every Aurora Micro 6DOF Sensor expressed in EM-system were saved 40 times ($n = 40$). The mean position for every Aurora Micro 6DOF Sensor (${}^{EM}\overline{\mathbf{p}}_k$) was calculated using Eq. 3.8. The transformation matrix ${}^{CT}\mathbf{T}_{EM}$ was multiplied with the position of every Aurora Micro 6DOF Sensor in order to express the position in CT-system (${}^{CT}\hat{\mathbf{p}}_k$), using Eq. 3.9.

The ED between the transformed positions expressed in CT-system by means of 3D tracked US registration (${}^{CT}\hat{\mathbf{p}}_k$ consisting of ${}^{CT}\hat{x}_k, {}^{CT}\hat{y}_k, {}^{CT}\hat{z}_k$), and the actual positions (${}^{CT}\overline{\mathbf{p}}_k$ consisting of ${}^{CT}\overline{x}_k, {}^{CT}\overline{y}_k, {}^{CT}\overline{z}_k$), was calculated for the five Aurora Micro 6DOF Sensors, using Eq. 3.10. Thereafter, the TRE expressed as RMSE was calculated, using these five ED and the Eq. 3.11.

This 3D tracked US protocol was repeated two more times.

3.3 Results

The positions of the Aurora Micro 6DOF Sensors saved before and after the CBCT were significantly different, where $p<0.002$ for repeat 1, 2 and 3. The biggest mean difference was 0.014 mm. The positions saved after CBCT were used for further calculation.

The TRE for the five Aurora Micro 6DOF Sensors after CBCT registration were 1.98 mm for repeat 1, 2.10 mm for repeat 2 and 2.02 mm for repeat 3, see Table 3.1.

Table 3.1: Target registration error of the CBCT registration protocol.

	Repeat 1	**Repeat 2**	**Repeat 3**
TRE (mm)	1.98	2.10	2.02

The sweeping times for the four different US sweeps are shown in Table 3.2.

Table 3.2: Sweeping time for the four different US sweeps.

	Repeat 1 Sweep time (s)	**Repeat 2 Sweep time (s)**	**Repeat 3 Sweep time (s)**
Left ilium and iliac crest	18	16	10
Right ilium and iliac crest	14	14	16
Os Pubis	14	9	11
U Turn	26	30	30

The TRE for the five Aurora Micro 6DOF Sensors after 3D tracked US registration are described in Table 3.3. The TRE of the 3D tracked US registration using the left and right iliac crest was high in repeat 3 (176.42 mm), compared to repeat 1 (2.24 mm) and repeat 2 (2.25 mm). The segmentation of repeat 3 contains gaps, see Figure 3.3a, while this is not observed for repeat 1 and 2. Secondly, all segmentations of the ilium show holes, see Figure 3.3b

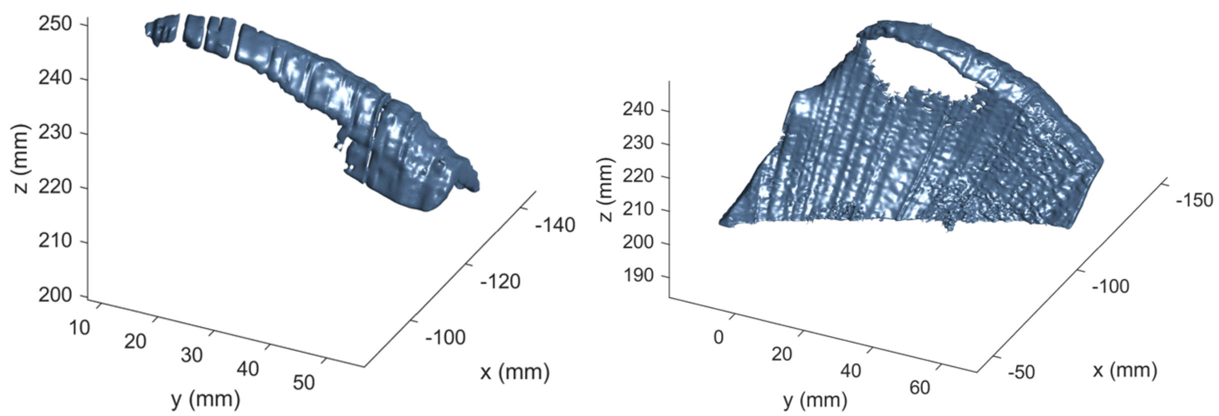

(a) Left iliac crest, with gaps in the segmentation

(b) Left ilium, with hole in the segmentation just below the iliac crest

Figure 3.3: Segmentation of the hip bones with gaps and hole

Table 3.3: Target registration error of the 3D tracked US registration protocol

Anatomy		Repeat 1 TRE (mm)	Repeat 2 TRE (mm)	Repeat 3 TRE (mm)
1	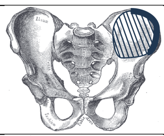	97.81	115.94	116.86
2	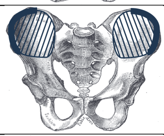	46.94	51.38	3.76
3	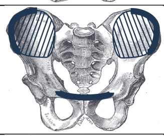	1.68	2.86	2.68
4	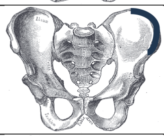	120.05	133.06	132.02
5	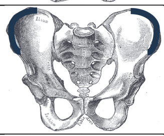	2.24	2.25	176.42
6	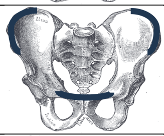	1.49	1.72	1.58
7	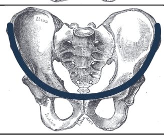	1.50	1.43	2.04

3.4 Discussion

The aim of this study was to determine the accuracy of surgical navigation using 3D tracked US registration compared to CBCT registration.

The paired T-test reveals a significant difference in the positions of the Aurora Micro 6DOF Sensors expressed in EM-system saved before and after the CBCT scans. However, the mean differences were 0.014 mm or less. In the current clinical practice, these differences do not influence the accuracy in such a way that is clinically relevant.

The TRE of CBCT registration is approximately 2 mm in this phantom study, see Table 3.1. The TRE in clinical setting is 4.0 mm [38]. The mobility of a patient is higher in clinical setting compared to the created phantom, resulting in inaccuracies and a higher TRE. The TRE of 2 mm will be used for comparison with the 3D tracked US registration, since both results are calculated with help of this phantom study

3D tracked US registration with the segmentations 3, 6 and 7 (Table 3.3) have comparable TRE to CBCT registration. This indicates a lot of potential for 3D tracked US registration. Furthermore, the TRE of segmentation 5 also indicates a lot of potential. However, the result of the repeat 3 is quite striking. This high TRE might be caused by sweeping the US beam too fast over the left iliac crest, resulting in gaps in the 3D US volume. Consequently, these gaps are also present in the segmentation, see Figure 3.3a. A segmentation consists of data points following the contour of a segmented object, in this case the bone. When there are gaps in the segmentation of the bone, data points are placed inside the anatomy of the bone. Consequently, the ICP algorithm struggles to link these data points of the US segmentation to the segmentation from CT imaging. A possible solution might be to use a single line of data points to indicate the bone surface on US, so it forms a shell instead of a contour.

3D tracked US registration with the segmentations 1 and 2 (Table 3.3) is not accurate. The ICP algorithm does not perform well, due to the hole in the US segmented bone (Figure 3.3b). The bone did not disappear, but the US was not able to "see" the bone due to an artefact called bone shadow (Figure 1.10a). When the sound waves reach the bone surface, they can not penetrate any further. Thus, leaving the area behind the first encountered bone surface in a "shadow". This results in missing and misplaced vertices, causing the ICP algorithm to fail in finding an adequate match. A possible solution might be to fill the hole, or only use the iliac crest for registration.

From Table 3.3 it is apparent that registration with a single side 3D tracked US, in this case the left side, is not accurate. Pre-processing before the registration might improve the TRE, when a region of interest is defined in CT imaging where we expect the US segmentation to be. In this case, the region of interest would be located at the upper left side of the pelvic bone.

As mentioned above, sweeping the US beam too fast over the anatomy causes gaps in the 3D US volume. CustusX is not able to interpolate between 2D slices, which are too far apart. The left ilium with iliac crest was sweeped in 18 seconds during repeat 1, 16 seconds during repeat 2 and 10 seconds during repeat 3. There are no gaps in repeat 1 and 2. Therefore, it is advised to take approximately 16 seconds for sweeping the left ilium with iliac crest at a constant speed and a frame rate of at least 20 frames/seconds. The right ilium with iliac crest could also be imaged in approximately 16 seconds at a constant speed and a frame rate of at least 20 frames/second. Furthermore, the os pubis was sweeped in 14 seconds during repeat 1, 9 seconds during repeat 2 and 11 seconds during repeat 3. There were no gaps in the data observed. Therefore, it is advised to sweep the os pubis area in approximately 9 seconds at a constant speed and a frame rate of at least 20 frames/second. The U-turn took 26 seconds during repeat 1, 30 seconds during repeat 2 and repeat 3. No gaps in the data were observed. So, it is advised to sweep the left ilium with iliac crest, os pubis and right ilium with iliac crest in approximately 25 seconds at a constant speed and a frame rate of at least 20 frames/second. This is an indication, but further research is necessary, to find the optimal sweep time in a clinical setting.

The positions of the Aurora Micro 6DOF Sensors expressed in CT-system were stated as reference points. It is not clear where exactly the signal of the sensors need to be indicated on CT-imaging. This might cause inaccuracies.

The segmentation method used in this experiment could not be used in the clinical setting. The phantom does not contain subcutaneous or muscle layers. These layers cause high intensities on the US imaging, similar to that of the bone. Segmentation through thresholding was possible due to the lack of these layers in the phantom. For clinical implementation another segmentation method for the bone segmentation in US imaging needs to be used.

3.5 Conclusion

This phantom study shows that surgical navigation with 3D tracked US registration has a lot of potential. The found TRE of 3D tracked US registration is comparable to the CBCT registration, when the segmented left and right iliac crest together with the os pubis are used for the registration. Pre-processing of the data might be a solution, when only the left and/or right iliac crest segmentations are used for registration. Sweeping the US beam too fast over the anatomy must be prevented, because gaps in the segmentation negatively influence the registration results. Before clinical implementation, further research is necessary, especially focused on bone segmentation in US imaging.

4 Discussion

In this study a new workflow is proposed and evaluated enabling laparoscopic surgical navigation for colorectal cancer patients without using a hybrid operating room.

After the experiments, the head of the sterilisation department revised his decision that Nylon PA2200 was sterilisable. Attaching the clip on with the EH-ACE is not intuitive, there are multiple ways to assemble. An industrial design student proposed a design were the sleeve consisted of two parts with a separate sensor holder [47]. The design is more intuitive and there is only a single way to assemble. The used material is Dental SG Resin, which the head of the sterilisation department approved to be cleaned, sterilised and reused.

It is expected that the new design will receive similar results on behalf of the accuracy inside the entire workfield, because the Aurora 6DOF Cable Tool is located in approximately the same location. Furthermore, the tracking accuracy during activation of the ultrasonic device will be similar, because the same laparoscopic instrument will be used. However, the dimensions of the new design might variate due to a different 3D printer, print technique and different material. The sliding mechanism of the two part sleeve might cause inaccuracies. Therefore, it is advised to repeat the calibration experiment, in order to validate the chosen calibration method.

Using the current clip-on there was no significant difference between the three calibration options. Therefore, the calibration with the most applicability is chosen, where only a single calibration is required for all clip-on EH-ACE combinations. No extra calibration is needed before the operation, saving OR time and cost. To ensure the validity of the calibration, a randomly selected clip-on should be tested per batch. If the accuracy is insufficient, the calibration can be revised.

The accuracy measurements in the TTFG workfield showed that the accuracy of EM tracking with the clip-on is adequate for almost the entire workfield of the TTFG. At the top level of the TTFG workfield the accuracy decreases, care should be taken to avoid this level when navigating. The surgeon is focused on the surgery and might fail to notice when the instrument enters this level. Therefore, a warning should be incorporated into the software when the EM sensor enters the top level of the TTFG workfield.

The activation of the EH-ACE does not seem to influence the accuracy of tracking with the clip-on. Allowing the surgeon to use the navigation during and directly after activation of the EH-ACE. The surgeon does not need to wait for any disturbances to disappear. Therefore, navigation is available throughout the entire surgery.

Laparoscopic surgery has a steep learning curve [48]. It is difficult to transform the information on the 2D display into 3D space. Surgical navigation with the clip-on provides the position and orientation of the EH-ACE compared to important anatomical structures in a 3D view. This supplementary information might help a novice laparoscopic surgeon to make the translation between the position on the 2D screen to the position in 3D space. Even for more advanced laparoscopic surgeons surgical navigation with the clip-on could be beneficial. For instance, when the tumour does not have a clear colour difference on the 2D screen or is occluded by other tissue, then the surgeon can turn to the navigation.

Surgical navigation using 3D tracked US registration has a lot of potential according to the phantom study. Before this method can be implemented in the clinical setting some adaptions need to be made. The BMI of the patient is of great importance in order to let the registration with 3D tracked US succeed. Patient with a high BMI have a lot of fat around the hip bones. In order to get a clear scan of the hipbones, pressure needs to be applied, this can cause movement and thus inaccuracies. Patients with a low BMI can have difficulties when scanning the os pubis. The os pubis can not be imaged, when the distance between the US probe and the bone is too small. A solution might be to place US transmitting material between the bone and the probe. Another solution to image the hipbones might be to scan the lateral sides of the patient. The problem of this solution is that the patient most often is bigger than the width of the TTFG workfield. When imaging the lateral side of the patient, the tracked US probe is located outside the TTFG workfield, where no data can be acquired. It needs to be evaluated if the TTFG can be rotated by 90 degrees for the registration and afterwards repositioned for the tracking during the operation.

Manual segmentation of the bones within the US imaging is too time consuming to be performed during a surgical procedure. Therefore, an automatic segmentation method needs to be developed before clinical implementation. A possible solution might be machine learning. The high intensity of the bone with the shadow region beneath are possible features for machine learning. The machine learning will eventually give a faster segmentation and more reproducible result.

Currently, registration with the 3D tracked US within a clinical setting is not yet possible. However, when a faster automatic segmentation method is developed and positively evaluated, then surgical navigation can also be performed without a hybrid operating room. Medical personal and patients will receive less radiation. The qualifications for operating an US machine are a lot less compared to the radiation emitting CBCT. Registration with 3D tracked US makes implementation of surgical navigation easier for (smaller) hospitals.

Bibliography

[1] World Cancer Research Fund International, *Colorectal cancer statistics*, 2018. [Online]. Available: https://www.wcrf.org/dietandcancer/cancer-trends/colorectal-cancer-statistics (visited on Jul. 2, 2019).

[2] Nederlandse Kankerregistratie, *IKNL*, 2011. [Online]. Available: https://www.cijfersoverkanker.nl/ (visited on Jul. 2, 2019).

[3] S. M. e. Silva, V. F. Rosa, A. C. N. dos Santos, *et al.*, „Influence of patient age and colorectal polyp size on histopathology findings.“, *Arquivos brasileiros de cirurgia digestiva*, vol. 27, no. 2, pp. 109–13, 2014.

[4] H. Gray and L. W. Harmon, *Anatomy of the Human Body*, 20th ed. Philadelphia: Lea & Febiger, 1918.

[5] B. Levin, P. Rozen, S. J. Spann, and G. P. Youngh, *Colorectal Cancer in Clinical Practice: Prevention, Early Detection and Management*. Oxfordshire: Taylor and Francis Group, 2005, p. 192.

[6] A. Berendsen and S. Van Belle, *Oncologie*. Houten: Bohn Stafleu van Loghum, 2017.

[7] U. Testa, E. Pelosi, and G. Castelli, „Colorectal Cancer: Genetic Abnormalities, Tumor Progression, Tumor Heterogeneity, Clonal Evolution and Tumor-Initiating Cells“, *Medical Sciences*, vol. 6, no. 2, p. 31, 2018.

[8] G. Brown, R. Reznek, and J. Husband, *Colo-Rectal Cancer*. Cambridge: Cambridge University Press, 2007.

[9] National Institute for Public Health and the Environment, *Bowel cancer screening program*. [Online]. Available: https://www.rivm.nl/en/bowel-cancer-screening-programme (visited on Jul. 29, 2019).

[10] Federatie Medisch Specialisten, *Richtlijnen database - colorectal cancer*, 2014. [Online]. Available: https://richtlijnendatabase.nl/en/richtlijn/colorectal%7B%5C_%7Dcancer/crc%7B%5C_%7D-%7B%5C_%7Dscreening.html (visited on Jul. 2, 2019).

[11] S. Gearhart and N. Ahuja, *Early Diagnosis and Treatment of Cancer Series: Colorectal Cancer*. Philadelphia: Saunders Elsevier, 2011.

[12] Colorectal Cancer Alliance, *Understanding a diagnosis by stage*. [Online]. Available: https://www.ccalliance.org/colorectal-cancer-information/stage-of-diagnosis (visited on Jul. 15, 2019).

[13] A. M. McCombie, F. Frizelle, P. F. Bagshaw, *et al.*, „The ALCCaS Trial“, *Diseases of the Colon & Rectum*, vol. 61, no. 10, pp. 1156–1162, 2018.

[14] W. Schwenk, B. Böhm, and J. M. Müller, *Postoperative pain and fatigue after laparoscopic or conventional colorectal resections: A prospective randomized trial*, 1998.

[15] Eurostat Statistics, *Surgical operations and procedures performed in hospitals*, 2017. [Online]. Available: `http://appsso.eurostat.ec.europa.eu/nui/submitViewTableAction.do` (visited on Apr. 30, 2018).

[16] S. W. Lee, „Laparoscopic procedures for colon and rectal cancer surgery“, *Clinics in Colon and Rectal Surgery*, vol. 22, no. 4, pp. 218–224, 2009.

[17] M. E. Trejo-Ávila, C. Valenzuela-Salazar, J. Betancourt-Ferreyra, *et al.*, „Laparoscopic Versus Open Surgery for Abdominal Trauma: A Case-Matched Study“, *Journal of Laparoendoscopic & Advanced Surgical Techniques*, vol. 27, no. 4, pp. 383–387, 2017.

[18] M. H. G. M. van der Pas, E. Haglind, M. A. Cuesta, *et al.*, „Laparoscopic versus open surgery for rectal cancer (COLOR II): Short-term outcomes of a randomised, phase 3 trial“, *The Lancet Oncology*, vol. 14, no. 3, pp. 210–218, 2013.

[19] J. Q. Cai, K. Chen, Y. P. Mou, *et al.*, „Laparoscopic versus open wedge resection for gastrointestinal stromal tumors of the stomach: A single-center 8-year retrospective cohort study of 156 patients with long-term follow-up“, *BMC Surgery*, vol. 15, no. 1, pp. 1–10, 2015.

[20] M. Laudicella, B. Walsh, A. Munasinghe, and O. Faiz, „Impact of laparoscopic versus open surgery on hospital costs for colon cancer: A population-based retrospective cohort study“, *BMJ Open*, vol. 6, no. 11, 2016.

[21] P. Małczak, M. Mizera, G. Torbicz, *et al.*, „Is the laparoscopic approach for rectal cancer superior to open surgery? A systematic review and meta-analysis on short-term surgical outcomes“, *Videosurgery and Other Miniinvasive Techniques*, vol. 13, no. 2, pp. 129–140, 2018.

[22] M. Keskin, M. Akici, O. Ağcaoğlu, *et al.*, „Open Versus Laparoscopic Surgery for Rectal Cancer: Single-Center Results of 587 Cases“, *Surgical Laparoscopy, Endoscopy and Percutaneous Techniques*, vol. 26, no. 3, e62–e68, 2016.

[23] R. Bogdanova, P. Boulanger, and B. Zheng, „Depth perception of surgeons in minimally invasive surgery“, *Surgical Innovation*, vol. 23, no. 5, pp. 515–524, 2016.

[24] M. Zelhart and A. M. Kaiser, „Robotic versus laparoscopic versus open colorectal surgery: towards defining criteria to the right choice“, *Surgical Endoscopy*, vol. 32, no. 1, pp. 24–38, 2017.

[25] T. Koivukangas, J. P. Katisko, and J. P. Koivukangas, „Technical accuracy of optical and the electromagnetic tracking systems“, *SpringerPlus*, vol. 2, no. 1, pp. 1–7, 2013.

[26] G. Xiao, E. Bonmati, S. Thompson, *et al.*, „Electromagnetic Tracking in Imaging-Guided Laparoscopic Surgery: Comparison with Optical Tracking and Feasibility Study of a Combined Laparoscope and Laparoscopic Ultrasound System“, *Medical Physics*, 2018.

[27] G. Zheng and S. Li, *3D Spatial Tracking*. Heidelberg: Springer Science+Business Media, 2016.

[28] E. Lugez, H. Sadjadi, D. R. Pichora, *et al.*, „Electromagnetic tracking in surgical and interventional environments: usability study“, *International Journal of Computer Assisted Radiology and Surgery*, vol. 10, no. 3, pp. 253–262, 2015.

[29] M. Li, „A robust electromagnetic tracking system for clinical applications“, *Curac*, no. March 2017, pp. 31–36, 2015.

[30] Nothern Digital Inc., *Aurora electromagnetic tracking system*, 2013. [Online]. Available: `http://www.ndigital.com/medical/wp-content/uploads/sites/4/2013/12/Aurora.pdf` (visited on Nov. 17, 2018).

[31] Northern Digital Inc., *Aurora Features*, 2019. [Online]. Available: `https://www.ndigital.com/medical/products/aurora/` (visited on Aug. 2, 2019).

[32] A. M. Franz, A. Seitel, M. Servatius, *et al.*, „Simplified development of image-guided therapy software with MITK-IGT“, D. R. Holmes III and K. H. Wong, Eds., Feb. 2012, 83162J. [Online]. Available: `http://proceedings.spiedigitallibrary.org/proceeding.aspx?doi=10.1117/12.911421`.

[33] J. Nijkamp, B. Schermers, S. Schmitz, *et al.*, „Comparing position and orientation accuracy of different electromagnetic sensors for tracking during interventions“, *International Journal of Computer Assisted Radiology and Surgery*, vol. 11, no. 8, pp. 1487–1498, 2016.

[34] D. Pandey, C. F. Yen, C. L. Lee, and M. P. Wu, „Electrosurgical technology: Quintessence of the laparoscopic armamentarium“, *Gynecology and Minimally Invasive Therapy*, vol. 3, no. 3, pp. 63–66, 2014.

[35] R. P. Blackstone, T. Bartley Pickron, and R. K. Zurawin, *Intelligent Ultrasonic Energy Delivered by HARMONIC® devices with Adaptive Tissue Technology*. [Online]. Available: `https://www.jnjmedicaldevices.com/en-US/product/harmonic-ace7-shears-advanced-hemostasis` (visited on Jul. 29, 2019).

[36] R. W. Timm, R. M. Asher, K. R. Tellio, *et al.*, „Sealing vessels up to 7 mm in diameter solely with ultrasonic technology“, *Medical Devices Evidence and Research*, pp. 263–271, 2014.

[37] Johnson and Johnson Medical N.V., *Harmonic ACE®+ Shears with Adaptive Tissue Technology*, 2019. [Online]. Available: `https://www.jnjmedicaldevices.com/en-US/product/harmonic-ace-shears-adaptive-tissue-technology` (visited on Jul. 29, 2019).

[38] J. Nijkamp, K. F. Kuhlmann, O. Ivashchenko, *et al.*, „Prospective study on image-guided navigation surgery for pelvic malignancies“, *Journal of Surgical Oncology*, vol. 119, no. 4, pp. 510–517, 2019.

[39] P. Laugier and G. Haïat, *Introduction to the physics of Ultrasound*. Heidelberg: Springer Science+Business Media, 2010.

[40] L. E. Bø, E. F. Hofstad, F. Lindseth, and T. A. Hernes, „Versatile robotic probe calibration for position tracking in ultrasound imaging“, *Physics in Medicine and Biology*, vol. 60, no. 9, pp. 3499–3513, 2015.

[41] L. Noltes, „Electromagnetic Tracking for Laparoscopic Instruments“, PhD thesis, University of Twente, 2018.

[42] D. C. Hoaglin and B. Iglewicz, „Rules for Some Resistant Outlier Labeling“, *Journal of the American Statistical Association*, vol. 82, no. 400, pp. 1147–1149, 1987.

[43] T. Hankel, „The development of a tracked laparoscopic tool during navigation“, University of Twente, Tech. Rep., 2018.

[44] Johnson and Johnson Medical N.V., *User guide G11 Endosurgery*, 2016. [Online]. Available: `https://www.jnjmedicaldevices.com/en-US/product/ethicon-gen11-generator` (visited on Jul. 29, 2019).

[45] ——, *Harmonic ACE®+ 7 Shears with Advanced Hemostasis*, 2016. [Online]. Available: `https://www.jnjmedicaldevices.com/en-US/product/harmonic-ace7-shears-advanced-hemostasis` (visited on Jul. 29, 2019).

[46] ——, *Harmonic Hand Pieces*, 2019. [Online]. Available: `https://www.jnjmedicaldevices.com/en-EMEA/product/harmonic-hand-pieces` (visited on Jul. 4, 2019).

[47] S. Bruseker, „A design to enable electromagnetic tracking on laparoscopic sealers/dividers for surgical navigation“, PhD thesis, University of Twente, 2019.

[48] G. Luglio, G. Domenico, D. Palma, *et al.*, „Laparoscopic colorectal surgery in learning curve : Role of implementation of a standardized technique and recovery protocol . A cohort study“, *Annals of Medicine and Surgery*, vol. 4, no. 2, pp. 89–94, 2015.